



A coupled hydro-mechanical creep damage model for clayey rock and its application to nuclear waste repository



S.P. Jia^{a,b,*}, L.W. Zhang^b, B.S. Wu^c, H.D. Yu^a, J.X. Shu^b

^a State Key Laboratory of Geomechanics and Geotechnical Engineering, Institute of Rock and Soil Mechanics, Chinese Academy of Sciences, Wuhan 430071, Hubei, China

^b Research center of Geomechanics and Geotechnical Engineering, Yangtze University, Jingzhou 434023, Hubei, China

^c CSIRO Energy, Melbourne 3168, Australia

ARTICLE INFO

Keywords:

Clayey rock
Permeability evolution
Damage
Hydro-mechanical coupling
Self-healing

ABSTRACT

In this paper we propose a new nonlinear elasto-viscoplastic damage model, based on a modified Mohr-Coulomb criterion, to study the creep and seepage in clayey rock during construction of a high-level radioactive waste repository through laboratory experiments and field tests. First, three types of damage evolution equations are constructed by using the relationship between the damage variable and the strain. Then, a self-healing model is investigated for the clayey rock by considering the damage, confining pressure, pore water, and duration of saturated state. By introducing the damage, permeability evolution and self-healing as the key factors, a fully coupled hydro-mechanical model for clayey rock is developed with the commercial software ABAQUS. The hydro-mechanical behaviour in the surrounding rock is simulated with the proposed model considering the actual construction of the repository. The numerical results show that the construction quality has a significant effect on the stability of the rock formation, and that the extent of the horizontal gallery disturbed by shield tunnelling is less than that of the test drift disturbed by using jackhammers method. The creep damage of the surrounding rock increases rapidly at the early stage and tends to stabilize gradually after 15 years, and the damage in the middle part of the surrounding rock is larger than that in the bottom and top parts. In addition, due to the self-healing effect of clayey rock, around three years later, the permeability of the excavation disturbed zone (EDZ) is close to that of the original clayey rock with an order of magnitude 10^{-19} m^2 . The present model can also be used to predict the long-term stability of tunnels.

1. Introduction

Characterization of hydro-mechanical coupling of rocks has become one of the most important topics in underground engineering (Kolditz et al., 2015) such as resource extraction, nuclear waste disposal and deep storage of natural gas or oil. Clayey rock, a class of soft rock that often causes instability problems in many underground engineering projects (Zhang and Rothfuchs, 2004; Fan et al., 2010; Yang et al., 2014; Liu et al., 2015), also involves this coupling process and particularly its creep properties are affected by the hydro-mechanical interaction. As underground engineering activities go deeper and deeper, the hydro-mechanical behaviours of clayey rock become more complicated because of damage evolution and pore fluid flowing in the disturbed rock mass (Wileveau and Bernier, 2008; Pardo et al., 2015; Lisjak et al., 2015). Furthermore, the permeability and fracture self-healing of disturbed rock are significantly affected by damage (Bastiaens et al., 2007; Zhang and Rothfuchs, 2008; Elkhoury et al.,

2015). Therefore, study on the hydro-mechanical coupling and time-dependent creep characteristics of clayey rock is of great interest and importance for physical repository design.

As one of the major soft rocks, clayey rock has obvious creep behaviour, which usually causes surrounding rock instability and supports structure failure in the tunnel, thus leading to high economic and environmental costs. Many researchers have investigated the creep characteristics of clayey rock through triaxial creep tests. It is found that there exist stress thresholds when the creep deformation occurs, and that different creep stages such as steady-state creep and accelerating creep have different stress thresholds. Although the creep behaviour of clayey rock has been widely investigated (Rejeb, 2003; Gasc-Barbier et al., 2004; Fabre and Pellet, 2006; Fan et al., 2010), there are few experimental studies under hydro-mechanical (HM) coupling conditions. Drained and undrained triaxial creep tests are most widely used for clayey rock. Extensive work has been conducted by the Belgian Agency for radioactive wastes management to characterize the creep behaviour

* Corresponding author at: State Key Laboratory of Geomechanics and Geotechnical Engineering, Institute of Rock and Soil Mechanics, Chinese Academy of Sciences, Wuhan 430071, Hubei, China.

E-mail address: jiashanporsm@163.com (S.P. Jia).

<https://doi.org/10.1016/j.tust.2018.01.026>

Received 19 February 2016; Received in revised form 13 April 2017; Accepted 20 January 2018

0886-7798/ © 2018 Elsevier Ltd. All rights reserved.

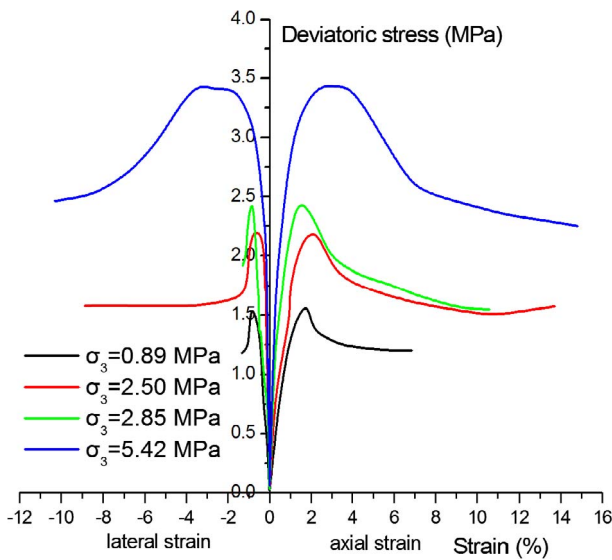


Fig. 1. Stress-strain curves of clayey rock under various confining pressures.

of Boom clay considering the HM interaction. Giraud and Rousset (1996) studied the creep behaviour under complex stress paths, and found that the creep deformation was significant under undrained conditions. Gong (2015) stated that the creep rate of clayey rock under drained condition was smaller than that under undrained condition. From the triaxial creep tests under HM coupling, Jia (2009) and Yu et al. (2015) found that there existed a deviatoric stress threshold below which no obvious creep was observed. When the deviatoric stress exceeds the threshold value, the creep deformation increases gradually with time, and the creep behaviour becomes more and more significant when the deviatoric stress increases. In addition, the mechanical properties of clayey rock are deteriorated by creep deformation and are nonlinearly dependent on the coupling of damage and hardening (Renner et al., 2000; Gasc-Barbier et al., 2004; Fabre and Pellet, 2006; Fan et al., 2010; Yu et al., 2015).

A proper creep constitutive model, which is capable of describing precisely the time-dependent deformation behaviours, is the key to the stability analysis of the clayey rock. Because the underground space has safety and environmental issues, a deep understanding of the rheological behaviours of clayey rock becomes vitally important. Existing time-dependent constitutive models include mainly the component rheological (CR) model, yield surface rheological (YSR) model, empirical rheological (ER) model, and endochronic rheological constitutive (ERC) model (Cristescu and Hunsche, 1998; Rejeb, 2003; Jia, 2009; Rutenberg and Lux, 2011). The CR model is the most popular one due to its simple concept and capability of revealing the rheological properties of rock. However, the predicted yield surface is static in the

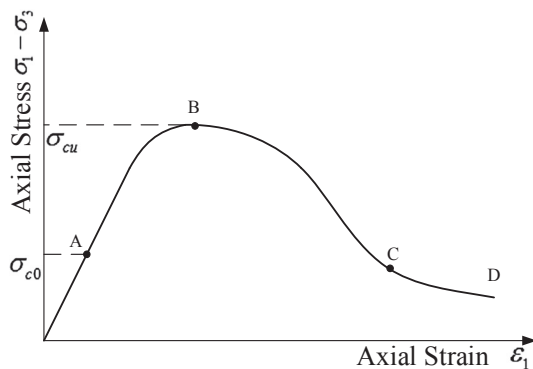


Fig. 2. Stress-strain curve of clayey rock in different stages.

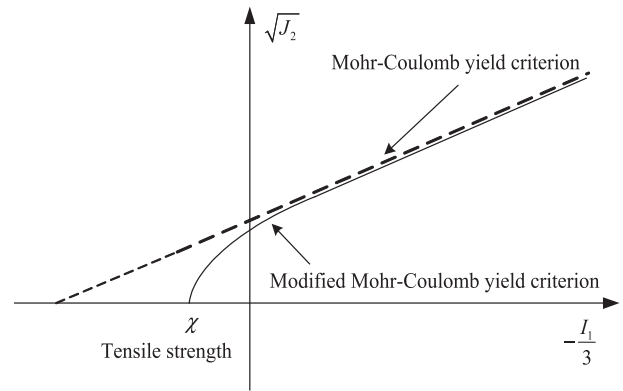


Fig. 3. Modified Mohr-Coulomb yield criterion.

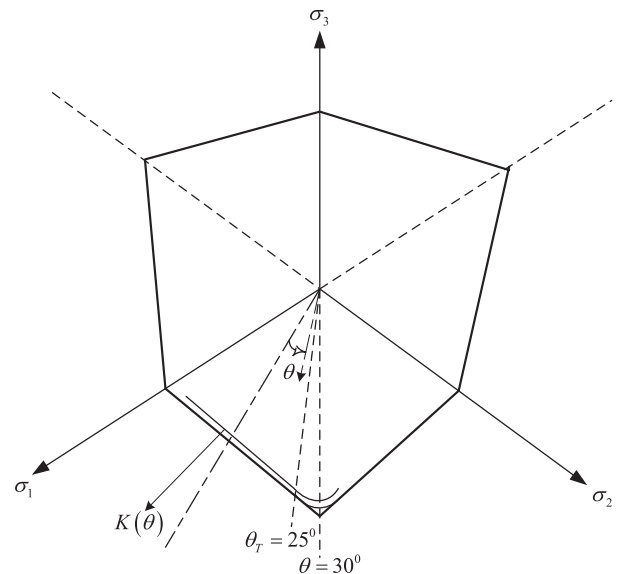


Fig. 4. Smooth treatment of Mohr-Coulomb criterion in the π plane.

CR model, which has the deficiency of fast creep convergence or accelerating creep. Compared to the CR model, the YSR model is more reasonable because the predicted yield surface changes dynamically with time. The ER model is able to explain the actual rheological behaviours under different stress paths, but it requires many creep tests to build. The ERC model can deal with not only static rheological behaviour, but also dynamic one under cyclic loading and unloading and

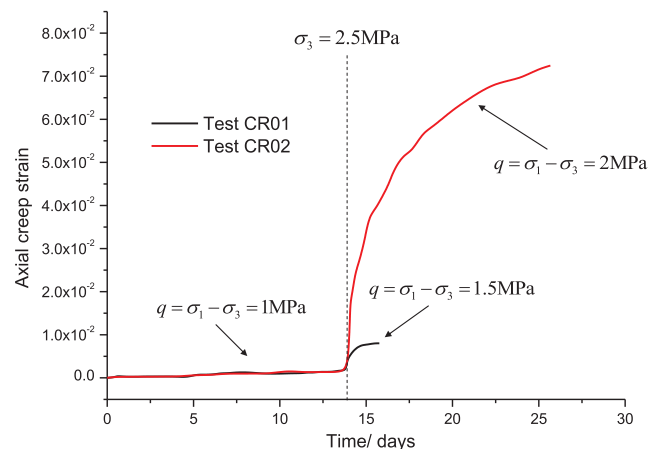


Fig. 5. Drained triaxial creep tests of clayey rock.

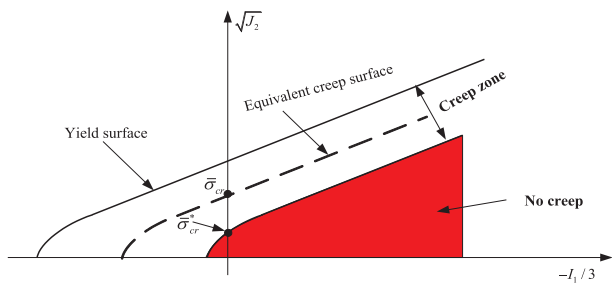


Fig. 6. Equivalent creep surface of Mohr-Coulomb criterion.

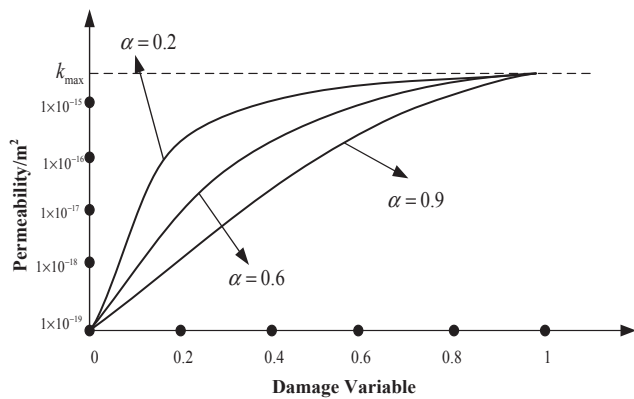


Fig. 7. Relationship between permeability and damage variable.

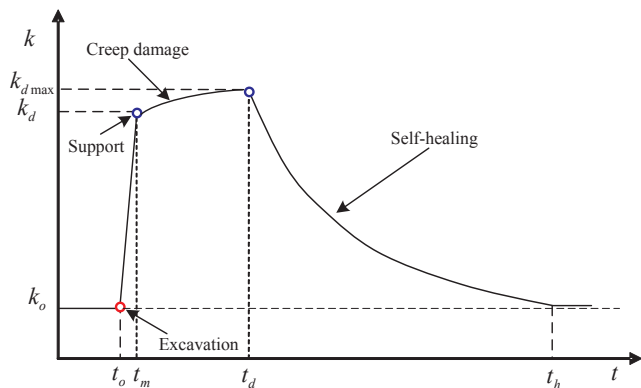


Fig. 8. Permeability evolution as a function of time.

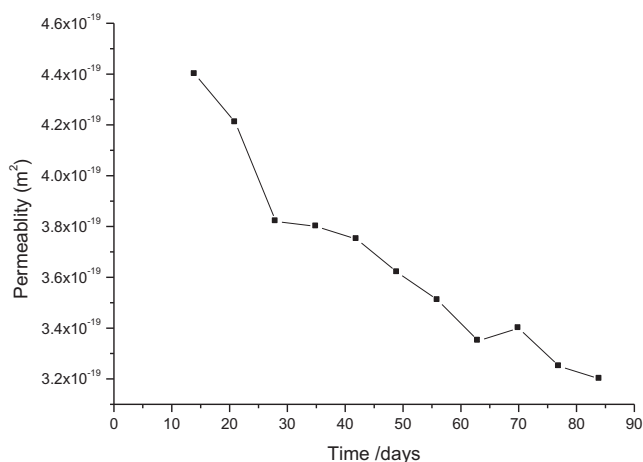


Fig. 9. Evolution of permeability of fractures in clayey rock as a function of time.



(a)



(b)

Fig. 10. Macroscopic fracture feature of clayey rock: after being exposed in the air for (a) 25 min and (b) 1 day.

vibration loading. Compared with the above models, the ERC model is less used because of its complex programming implementation.

A large number of engineering applications and laboratory tests show that damage is an important factor for the failure of rock mass, especially clayey rock (Hunsche and Hampel, 1999; Fabre and Pellet, 2006). The damage of clayey rock has obvious time-dependent characteristics. For example, it makes the rock deform nonlinearly and accumulates gradually, especially in the third creep stage or accelerated creep stage until the rock failure occurs (Jia, 2009; Yu et al., 2015). Most of the previous studies mainly focus on the creep characteristics and failure mechanism of clayey rock under different stress levels, but without considering the effect of pore pressure on the creep (Renner et al., 2000; Wang and Xu, 2013). The seepage process and pore pressure change make the mechanical behaviours of rock mass complicated. First, the pore pressure and deviatoric stress have a significant effect on

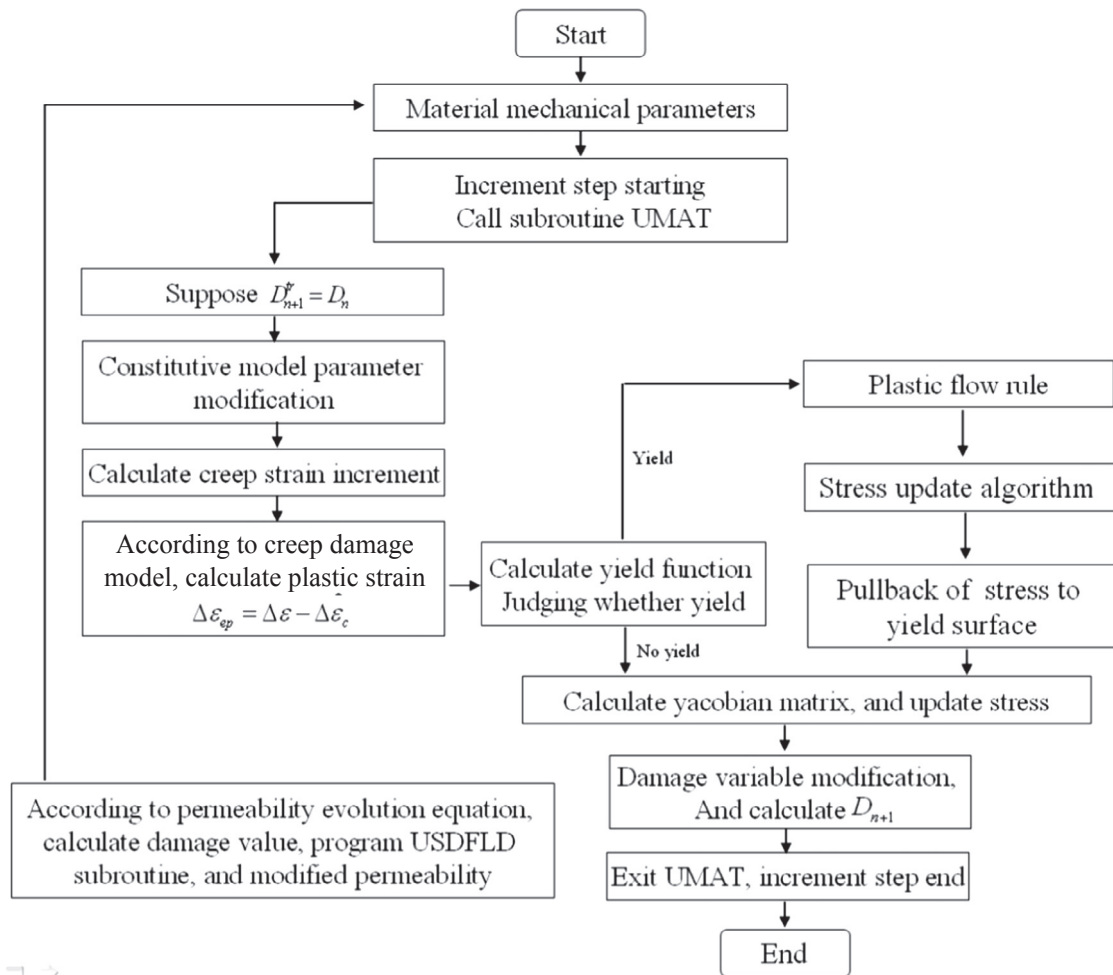


Fig. 11. Secondary development of creep and seepage coupled model.

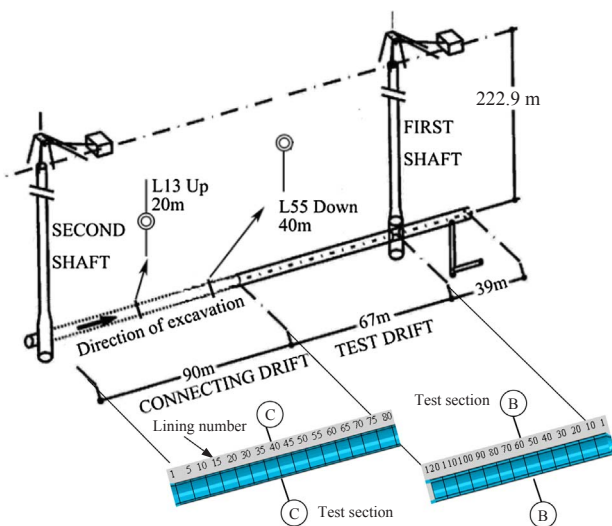


Fig. 12. Schematic overview of HADES, tunnel lining and test section.

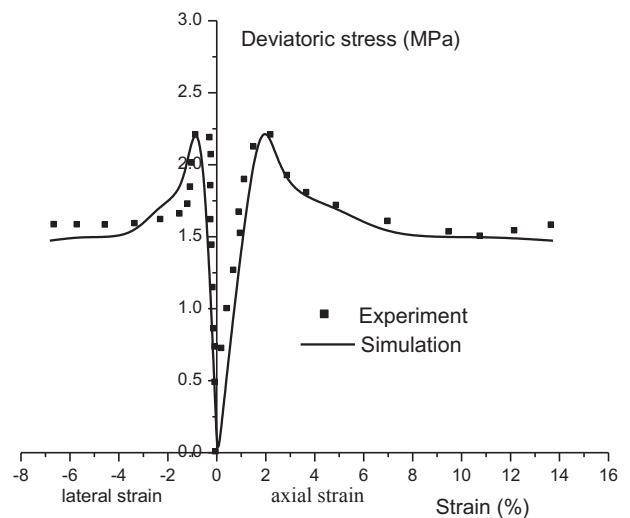


Fig. 13. The stress-strain curves of clayey rock under a confining pressure 2.5 MPa.

the elasticity modulus, cohesive strength and creep parameters which may change with seepage time. A quantitative relationship can be developed between the creep parameters, deviatoric stress, and pore pressure. Second, the creep deformation and rock damage influence the seepage capacity as the permeability and porosity are changed. Surrounding rock instability has become a serious problem in underground engineering for nuclear waste disposal, and some countries have built

large-scale underground laboratories (for example the Bure laboratory in France and Mol laboratory in Belgium) to study the coupled seepage-creep properties of clayey rock (Jia, 2009). Field data can provide a supplement to the laboratory creep tests concentrating on conventional triaxial condition.

The aim of the present work is to develop a coupled numerical model for studying the creep and seepage in clayey rock during

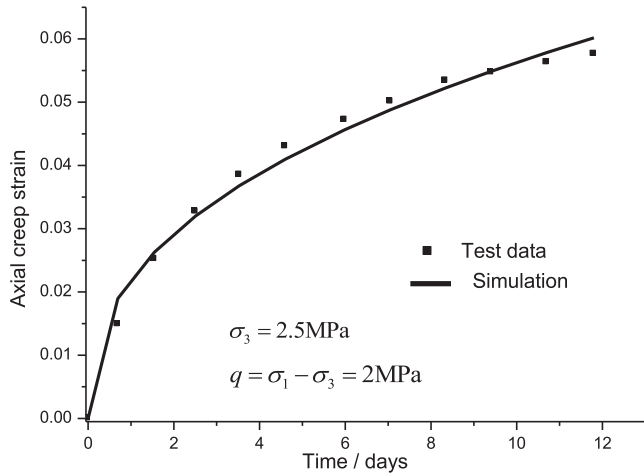


Fig. 14. Axial creep strain for the drained triaxial creep test.

excavation and construction process of a high-level radioactive waste repository. The effect of damage and self-healing of fractures on permeability change is also taken into account in this model. The remainder of this paper is organized as follows. Section 2 provides the formulation of the coupled model including the new yield criterion and constitutive laws for creep-damage and permeability and self-healing. For the purpose of clarity, the previous experimental or field results, based on which the new coupled model are formulated, are briefly summarized at the beginning of the each subsections. In Section 3 a second development combined with the commercial package is dealt with to solve the coupled model by using finite element method. The coupled model is applied to a physical project in Section 4, which is followed by a brief conclusion in Section 5.

2. Coupled model for the creep and seepage in clayey rock

2.1. Yield criterion

The yield criterion used in the present work is obtained based on the undrained shear tests performed under a confining pressure (CP) ranging from 0.89 MPa to 5.42 MPa (Jia, 2009). The stress-strain curves of clayey rock under different confining pressures are shown in Fig. 1. The deformation process is divided into four stages as shown in Fig. 2: (a) elastic deformation before initial yield stress σ_{c0} (A); (b) nonlinear deformation AB; (c) strain softening phase BC; and (d) plastic flow phase CD.

An elastoplastic damage model is developed to describe the stress-strain relationship of clayey rock. As the residual strain in the stage AB is very small, it can be ignored and thus an elastic damage model is used to describe the nonlinear behaviour for this stage. Then, a plastic damage model is used for the subsequent stages, i.e. strain softening and plastic flow, where the elastic stiffness, yield function and potential

function of clayey rock are updated by considering the plastic damage. Two assumptions are made in this elastoplastic damage model: (a) the compression strength of clayey rock meets the Mohr-Coulomb (MC) criterion during strain softening deformation; and (b) the residual strength also meets the MC criterion in the plastic flow stage CD.

As the conventional MC criterion overestimates the tensile strength of rock, we use a modified Mohr-Coulomb (MMC) yield criterion (Fig. 3) that considers the real tensile strength of clayey rock (Jia et al., 2010; Pardoen et al., 2015). The MMC yield function F is defined as follows (Muñoz, 2006)

$$F = \frac{I_1}{3} \sin \phi + \sqrt{J_2 K^2(\theta) + (c \cot \phi - \chi)^2 \sin^2 \phi} - c \cos \phi \quad (1)$$

where I_1 is the first stress invariant, J_2 is the second stress invariant, θ is the lode angle. χ , ϕ and c denote the tensile strength, friction angle and cohesion, respectively. $K(\theta)$ is a function defined later.

There are six corners in the conventional MC yield surface, which makes the computation difficult to converge. To make the MMC yield surface smooth, continuous and close to the conventional MC yield surface as shown in Fig. 4, a piecewise functions $K(\theta)$ is defined (Muñoz, 2006; Jia et al., 2010)

$$K(\theta) = \begin{cases} A - B \sin 3\theta, & \text{on } |\theta| > \theta_T \\ \cos \theta - 1 / \sqrt{3} \sin \phi \sin \theta & \text{on } |\theta| \leq \theta_T \end{cases} \quad (2)$$

where θ_T is equal to 25° considering the computational efficiency, and

$$A = \frac{1}{3} \cos \theta_T \left[3 + \tan \theta_T \tan 3\theta_T + \frac{1}{\sqrt{3}} \text{sign}(\theta) (\tan 3\theta_T - 3 \tan \theta_T) \sin \phi \right] \quad (3)$$

$$B = \frac{1}{3 \cos 3\theta_T} \left[\text{sign}(\theta) \sin \theta_T + \frac{1}{\sqrt{3}} \sin \phi \cos \theta_T \right] \quad (4)$$

$$\text{sign}(\theta) = \begin{cases} 1, & \theta \geq 0^\circ \\ -1, & \theta < 0^\circ \end{cases} \quad (5)$$

A damage surface function f^d is assumed to be in the strain space similar to a plastic yield surface. When the state point of stress is on the damage surface, the damage continues and the surface expands with the damage growth during the deformation process (Millard et al., 2009). The damage growth is controlled by the following criterion (Chiarelli et al., 2003; Jia, 2009)

$$\begin{cases} f^{de}(\tau, D_e) = \beta_1(\tau - \tau_0) - D_e \leq 0 \\ f^{dp}(\tau, D_p) = \frac{\tau - \tau_{0p}}{\alpha_2 + \beta_2(\tau - \tau_{0p})} - D_p \leq 0 \end{cases} \quad (6)$$

where $\tau = \sqrt{\varepsilon_{ij} \mathbf{E}_{ijkl} \varepsilon_{kl}}$ is the energy index with ε_{ij} being the strain tensor and \mathbf{E}_{ijkl} the elasticity matrix. τ_0 and τ_{0p} denote the thresholds of elastic damage, D_e , and plastic damage, D_p , respectively. β_1 is a model parameter for elastic damage, α_2 and β_2 are model parameters for plastic damage.

The plastic potential function G is determined from the above modified yield function

Table 1
Material and model parameters of clayey rock.

E (MPa)	μ	c (MPa)	ϕ ($^\circ$)	φ ($^\circ$)	τ_0 (MPa $^{1/2}$)	β_1	τ_{0p} (MPa $^{1/2}$)
300	0.13	0.3	18	2.88	0.227	0.86	0.362
η	α_2	β_2	$A_1/(10^{-4})$	B_1	C_1	n	ω
0.6	0.96	1.233	5.26	3.41	-0.46	3.1	0.39
$\bar{\sigma}_{cr}^*$ (MPa)	$k_{0h}/(10^{-19} \text{ m}^2)$	$k_{0v}/(10^{-19} \text{ m}^2)$	ξ	α	α_1	α_2	α_3
1.0	9.95	3.80	3.0	0.36	0.0105	0.101	0.585

Table 2
Material and model parameters of different lining.

Position	E (GPa)	μ	γ (kNm ⁻³)	k (10 ⁻¹⁸ m ²)
Shaft	35.0	0.3	25	0.00
Test	2.35	0.3	20	3.62
Connecting	49.24	0.3	25	1.10

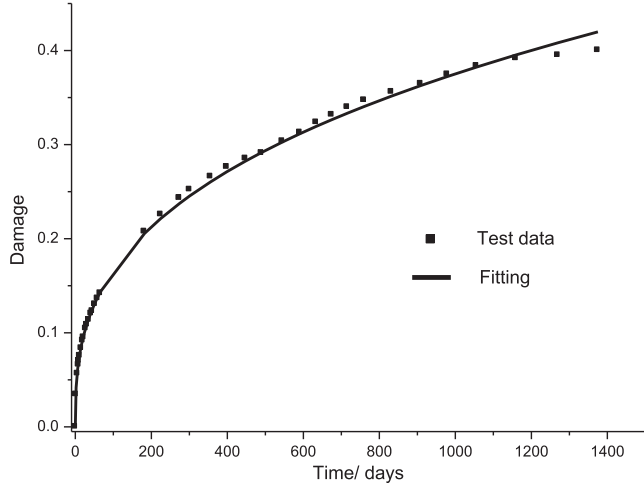


Fig. 15. Damage evolution curve of lining material.

$$G = \frac{I_1}{3} \sin \phi + \sqrt{J_2 K^2(\theta) + (c \cot \phi - \chi)^2 \sin^2 \phi} \quad (7)$$

where ϕ is the dilation angle of rock.

2.2. Creep damage model

The creep damage model to be developed is based on the drained triaxial creep tests performed under various deviatoric stress with a confining pressure close to the in-situ effective mean stress 2.5 MPa (Jia, 2009). The creep strain variation with time is shown in Fig. 5, where we find that there exists a deviatoric stress threshold between 1 and 1.5 MPa for the onset of creeping. When the deviatoric stress is larger than this threshold value, the creep deformation is activated and the creep rate will be dependent on time and accumulated creep deformation. However, when the stress level is low, the creep rate decays to zero very quickly and the creep deformation is so small that it can be neglected.

As mentioned above, the creep flow of clayey rock is consistent with its plastic flow. The equivalent creep surface is defined by homogeneously scaling down the yield surface (ABAQUS, 2004), which is parallel to the shear failure surface in the meridional plane as shown in Fig. 6. This creep surface consists of points that share the same creep intensity measured in terms of equivalent creep stress $\bar{\sigma}_{cr}$

$$\bar{\sigma}_{cr} = \frac{I_1}{3} \tan \phi + \sqrt{J_2 \frac{K^2(\theta)}{\cos^2 \phi} + (c \cot \phi - \chi)^2 \tan^2 \phi} \quad (8)$$

The creep deformation of clayey rock is nonlinear because of the continuous changing and rebuilding of its internal structure. The creep damage is the result of the internal cracks that have developed. The following creep damage criterion is used for clayey rock (Xie, 1990)

$$f^{dc}(\varepsilon_c, D_c) = \exp\left(\frac{\varepsilon_c}{\varepsilon_{cmax} \cdot \omega}\right) - 1 - \frac{D_c}{A_0} \leq 0 \quad (9)$$

where $A_0 = \exp(-1/\omega)$, ω is the model parameter. ε_c is creep strain, ε_{cmax} is the maximum creep strain, and D_c is the creep damage.

In order to characterize the complex creep deformation of clayey rock and the influence of seepage on the creep behaviour, a modified

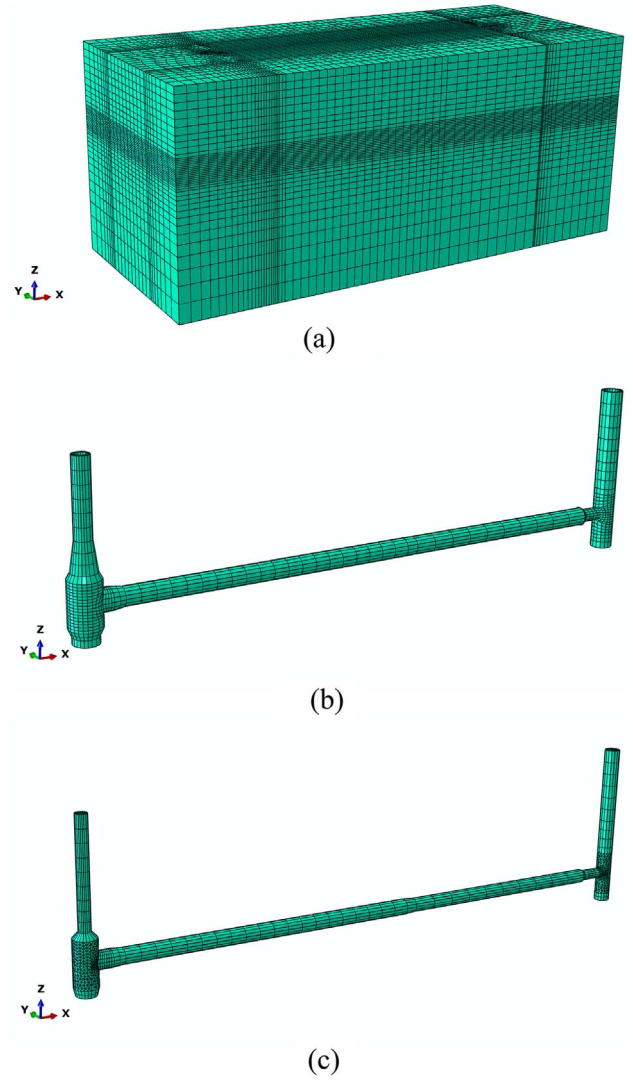


Fig. 16. Numerical model: (a) a view of the whole model, (b) shaft and lining model, and (c) excavation model.

empirical power function is used (Rejeb, 2003; Tian et al., 2015)

$$\begin{cases} \dot{\varepsilon}_c = A_1 (\bar{\sigma}_{cr})^n t^m H(\bar{\sigma}_{cr} - \bar{\sigma}_{cr}^*) / (1 - D_c) \\ m = B_1 \varepsilon_c + C_1 \end{cases} \quad (10)$$

where t is time, $\dot{\varepsilon}_c$ is the creep strain rate, A_1 , B_1 , C_1 and n are the model parameters, $\bar{\sigma}_{cr}^*$ is the threshold value of the equivalent creep stress, H is the Heaviside function. The parameter m determines which stage the creep deformation is at. When $-1 < m < 0$, $m = 0$ and $m > 0$, clayey rock is in the primary, secondary and tertiary creep stages, respectively.

To obtain the damage evolution equation in three-dimensional space, an equivalent creep strain $\bar{\varepsilon}_c$ is defined (Xie, 1990; Tian et al., 2015)

$$\begin{cases} \dot{\bar{\varepsilon}}_c = \sqrt{\frac{2}{3}} \dot{\varepsilon}_c \\ \bar{\varepsilon}_c = \int_0^t \dot{\bar{\varepsilon}}_c dt \end{cases} \quad (11)$$

where

$$\dot{\varepsilon}_c = \frac{\dot{\bar{\varepsilon}}_c}{f^{cr}} \left\{ \frac{\partial G}{\partial \sigma} \right\} \quad (12)$$

$$f^{cr} = \frac{1}{\bar{\sigma}_{cr}} \sigma \cdot \frac{\partial G}{\partial \sigma} \quad (13)$$

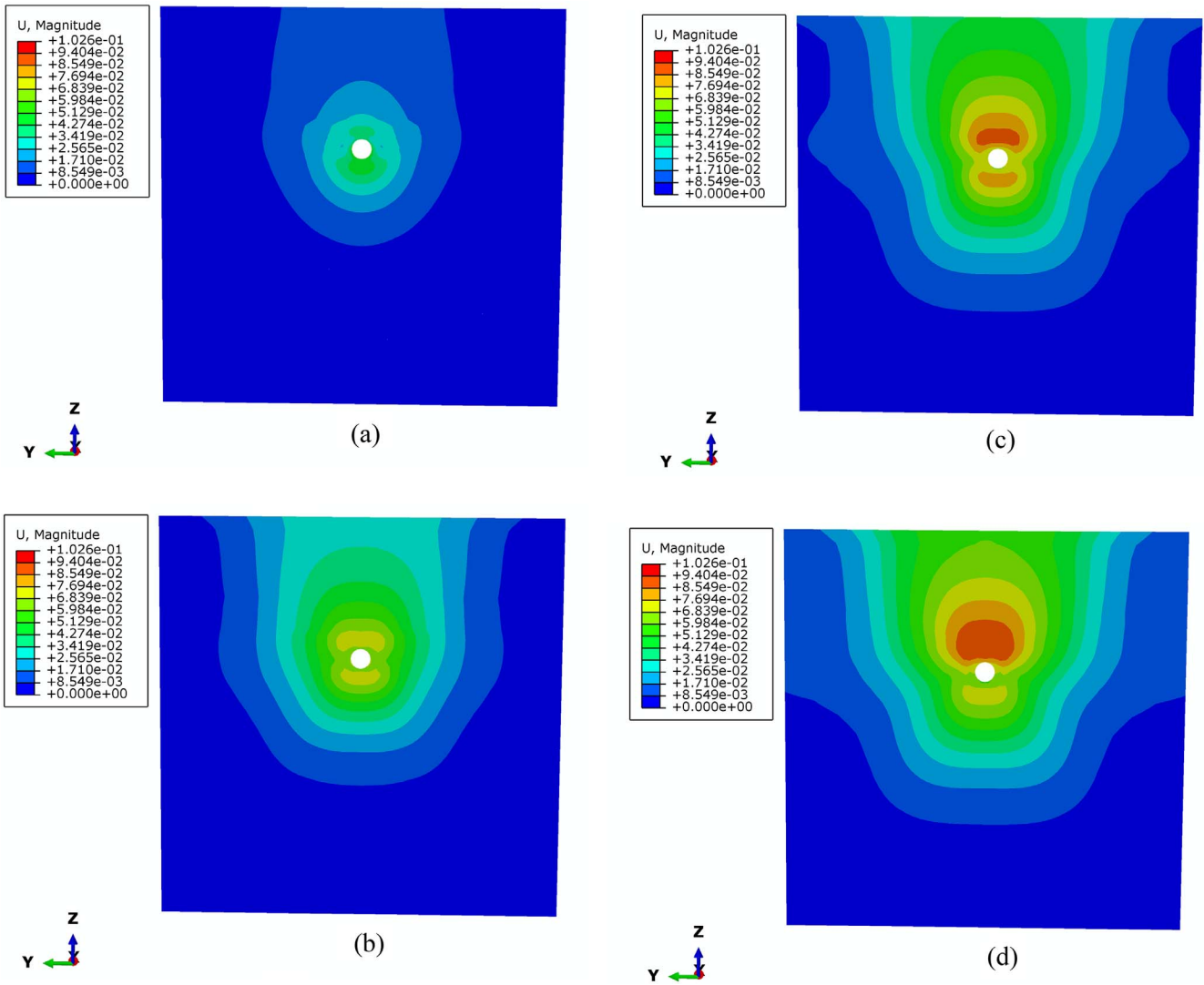


Fig. 17. Deformation distribution of Section B-B with time: (a) after the test drift was constructed, (b) 10 years after the test drift was constructed (since 1987), (c) after the connecting drift was constructed and (d) 10 years after the connecting drift was constructed (since 2002).

2.3. Permeability evolution by considering the damage and self-healing effect

Excavation unloading inevitably leads to stress redistribution, damage and permeability change in the surrounding rock. Many experiments on clayey rock show that (a) during elastic deformation, the permeability change is so small that it can be ignored; and (b) after that, the permeability will increase gradually and then rapidly when the initiation and propagation of cracks or damage occurs (Renner et al., 2000; Zhang and Rothfuchs, 2004; Hou and Lux, 2004; Li et al., 2011; Liu et al., 2015). After tunnel construction and lining supporting, the surrounding rock continues to deform with the coupling effect of creep and consolidation. Therefore, the creep damage of clayey rock increases gradually, so does the permeability at the early stage (Xu et al., 2012). The damage evolution is mainly affected by the unloading damage, D_m , resulting from excavation and the creep damage, D_c . In the excavation stage, the accumulated creep strain is very small under fast unloading and thus the transient unloading damage $D_m(\sigma,0)$ is the major factor (Hou and Lux, 2004; Muñoz, 2006; Li et al., 2011; Jia et al., 2015). However, the creep damage D_c cannot be ignored under slow or continuous loading after lining support. The evolution equation of damage-permeability is defined as follows (Fig. 7)

$$k_d = k_0 \cdot 10^{\xi(A'e^{-D_T/\alpha+B'})} \quad (14)$$

where k_0 is the initial rock permeability, ξ is the order of magnitude for increased permeability, α , A' and B' are model parameters, and $A' = -B' = (e^{-1/\alpha}-1)^{-1}$. The total damage D_T is defined by (Hou, 2003; Souley et al., 2011; Xu et al., 2012)

$$D_T = D_c(\sigma,t) + D_m(\sigma,0) = D_c + D_e + D_p \quad (15)$$

Many field and laboratory tests have shown that, due to significant self-healing effect of fractures in the saturated state, the permeability tends to be close to that of undisturbed clayey rock (Bastiaens et al., 2007; Li et al., 2011; Elkhoury et al., 2015; Jia et al., 2015). The self-healing of clayey rock is mainly related to the saturated time and stress state. The surrounding rock will return to the saturated state for a period of time after lining support. With increasing the radial compressive stress and reducing the deviatoric stress, the fractures tend to close and the permeability decreases gradually (Fig. 8).

The data from self-healing tests (Jia, 2009) is used to characterize the effect of self-healing on the permeability of clayey rock. In these tests, an artificial fracture was made to cross the axis of cylindrical samples, which were placed in the triaxial cell under saturated state. Fig. 9 shows the permeability evolution with time under a confining

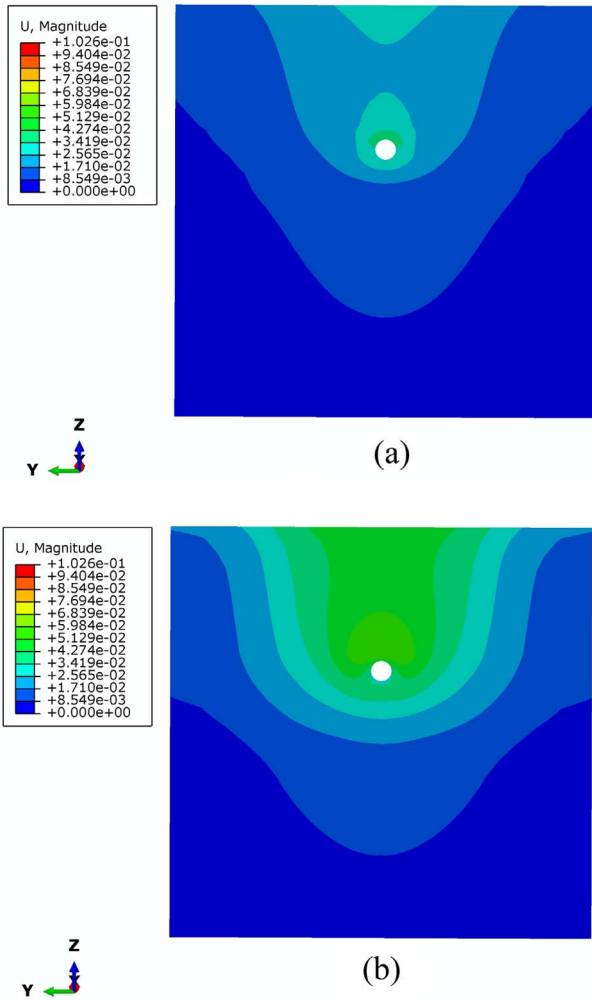


Fig. 18. Deformation distribution of Section C-C with time: (a) after the connecting drift was constructed and (b) 10 years after the connecting drift was constructed (since 2002).

pressure of 4.5 MPa. It can be seen that the permeability decreases roughly in exponential form with time because of the self-healing effect. When the sample was taken out of the triaxial cell, no macroscopic fracture was observed. However, after being exposed to the air for one day, one fracture could be observed. The longer the exposure time, the more obvious the fracture, as shown in Fig. 10.

The relationship between the permeability and the self-healing effect is described by the following equation (Li et al., 2011; Jia et al., 2015)

$$k = k_0 + (k_d - k_0)h(p, q, t) \quad (16)$$

where the self-healing factor $h(p, q, t)$ is defined as (Jia, 2009)

$$h(p, q, t) = \exp\left(-a_1 \frac{p^{a_2}}{q^{a_3}} t\right) \quad (17)$$

where a_1 , a_2 and a_3 are model parameters. p and q denote the hydrostatic pressure and Mises stress, respectively.

From Eqs. (16) and (17), the fractures are more likely to close and heal with high hydrostatic pressure and low deviatoric stress. The longer the saturated time is, the easier the self-healing becomes.

2.4. Discussion about the drained and undrained conditions due to excavation in clayey rock

In this study, the term “drained conditions” means that the pore fluid is allowed to flow into or out of the clayey rock. The response of

clayey rock due to excavation contains two phases: short-term response as a result of excavation and support and long-term response which could last for tens of years. Given the low permeability (for example 10^{-19} m^2) of clayey rock and relatively fast tunneling, the excavation response occurs under almost undrained conditions. The undrained condition is relevant to the water flow characteristics which are investigated for short-term response. Although the damaged zone will be partially drained (Mertens et al., 2004; Bastiaens et al., 2007), the clayey rock is assumed to deform in undrained condition immediately after excavation. Because of this, an undrained solution to the excavation problem of clayey rock galleries can be used (Labieuse and Giraud, 1998; Barnichon and Volckaert, 2003). Therefore, the undrained triaxial shear test can simulate the stress-strain state and measure the shear strength of saturated clayey rock for actual engineering conditions such as fast construction (Zhang and Rothfuchs, 2004; Yu et al., 2012).

As the permeability of linings is one order of magnitude larger than that of clayey rock (Li et al., 2011; Jia et al., 2015), drained condition is taken for the long-term stability analysis of the gallery. In addition, the drained triaxial creep tests can determine the creep parameters which are required for predicting the long-term HM behaviour of clayey rock under drained conditions.

3. Numerical method

3.1. Finite element formulation

According to the damage mechanics theory, the stress-strain equation is written as follows (Xie, 1990)

$$\sigma_{ij} = \tilde{\mathbf{E}}_{ijkl} \varepsilon_{kl}^c \quad (18)$$

where $\tilde{\mathbf{E}}_{ijkl}$ is the effective elasticity matrix, and ε_{kl}^c is the elastic strain tensor. The differential equation of Eq. (18) is (Hou, 2003; Souley et al., 2011)

$$d\sigma_{ij} = \tilde{\mathbf{E}}_{ijkl} (d\varepsilon_{kl} - d\varepsilon_{kl}^p - d\varepsilon_{kl}^c) + d\tilde{\mathbf{E}}_{ijkl} (\varepsilon_{kl} - \varepsilon_{kl}^p - \varepsilon_{kl}^c) \quad (19)$$

where $d\varepsilon_{kl}$, $d\varepsilon_{kl}^p$, $d\varepsilon_{kl}^c$ are the total strain increment, plastic strain increment and creep strain increment, respectively.

Suppose that the displacement and pore pressure of element nodes are $\{u\}_n^{(e)}$, $\{p\}_n^{(e)}$ and $\{u\}_{n+1}^{(e)}$, $\{p\}_{n+1}^{(e)}$ from time t_n to t_{n+1} , and the incremental displacement and pore pressure of element nodes are $\{\Delta u\}^{(e)}$, $\{\Delta p\}^{(e)}$ at time step $\Delta t_n = t_{n+1} - t_n$. According to virtual work principle, the element equilibrium equation for the rock skeleton in incremental form is (ABAQUS, 2004; Kolditz et al., 2015)

$$[\tilde{\mathbf{k}}_{uu}]^{(e)} \{\Delta u\}^{(e)} + [\mathbf{k}_{up}]^{(e)} \{\Delta p\}^{(e)} = \{\Delta \mathbf{f}\}^{(e)} + \{\Delta \mathbf{R}^p\}^{(e)} + \{\Delta \mathbf{R}^c\}^{(e)} + \{\Delta \mathbf{R}^d\}^{(e)} \quad (20)$$

where $[\tilde{\mathbf{k}}_{uu}]$ is the element stiffness matrix, $[\mathbf{k}_{up}]$ is the coupling matrix, $\{\Delta \mathbf{f}\}$ is the external load increment array, $\{\Delta \mathbf{R}^p\}$, $\{\Delta \mathbf{R}^c\}$ and $\{\Delta \mathbf{R}^d\}$ are the additional force arrays caused by plastic strain, creep strain and damage evolution, respectively.

The continuity equation for the fluid based on Darcy’s law is (Muñoz, 2006; Kolditz et al., 2015)

$$\frac{k_i}{\mu_f} p_{,ii} = \alpha_m \dot{p} + \alpha' \dot{\varepsilon}_{ii} + q_f \quad (21)$$

where k_i is the permeability of rock, μ_f is the fluid dynamic viscosity, α_m is the integrated compression factor of the porous media, α' is Biot coefficient, $\dot{\varepsilon}_{ii}$ is the volumetric strain rate and q_f is the fluid source.

Based on two types of seepage boundary conditions, i.e. constant pressure and constant flux, by using Galerkin method, the continuity equation for the fluid element is (ABAQUS, 2004; Kolditz et al., 2015)

$$[\mathbf{k}_{up}]^{(e)T} \{\dot{u}\}^{(e)} + [\mathbf{k}_p]^{(e)} \{\dot{p}\}^{(e)} + [\mathbf{k}_{pp}]^{(e)} \{p\}^{(e)} = \{\mathbf{Q}_f\}^{(e)} \quad (22)$$

where $[\mathbf{k}_p]$ is the fluid matrix, $[\mathbf{k}_{pp}]$ is the seepage matrix, and $\{\mathbf{Q}_f\}$ is the

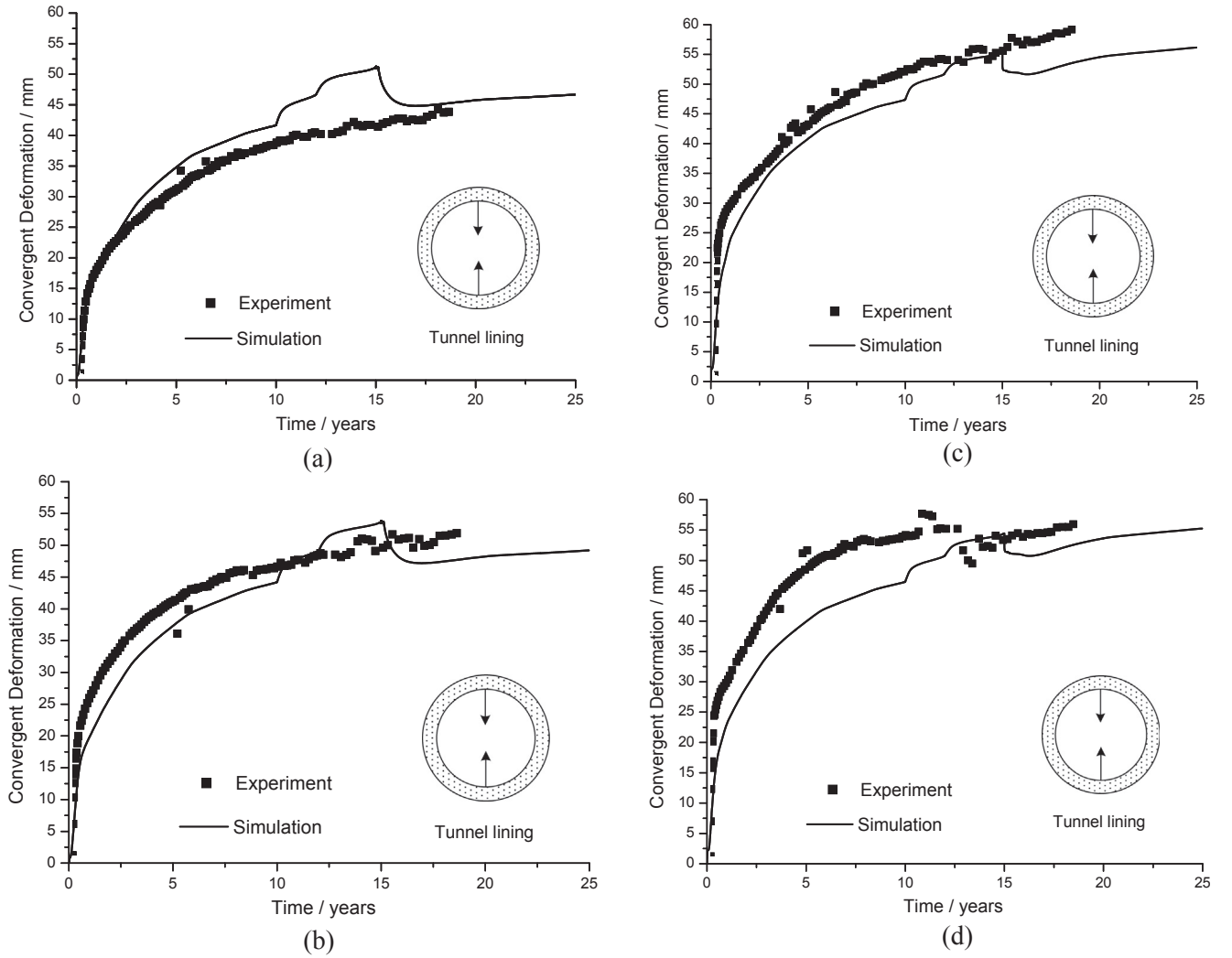


Fig. 19. Variation with time of convergent deformation of lining in the test drift for (a) L43, (b) L52, (c) L83 and (d) L105.

fluid source array.

As the continuity equation contains time derivative, the integration domain should be from t_n to t_{n+1} . By using the general form of integration of a variable with respect to time (Kolditz et al., 2015)

$$\int_{t_n}^{t_{n+1}} \{p\}^{(e)} dt \approx \Delta t_n [\vartheta \{p\}_{n+1}^{(e)} + (1-\vartheta)\{p\}_n^{(e)}] = \Delta t_n [\{p\}_n^{(e)} + \vartheta \{\Delta p\}^{(e)}] \quad (23)$$

where $\vartheta \in [0,1]$ is the time integration factor, Eq. (22) becomes

$$[\mathbf{k}_{up}]^{(e)T} \{\Delta u\}^{(e)} + ([\mathbf{k}_p]^{(e)} + \vartheta \Delta t [\mathbf{k}_{pp}]^{(e)}) \{\Delta p\}^{(e)} = \Delta t (\{Q_f\}^{(e)} + \vartheta \{\Delta Q_f\}^{(e)} - [\mathbf{k}_{pp}]^{(e)} \{p\}_n^{(e)}) \quad (24)$$

Therefore, the general equilibrium equation after combining all the elements is written as

$$\begin{bmatrix} \tilde{\mathbf{K}}_{uu} & \mathbf{K}_{up} \\ \mathbf{K}_{up}^T & \mathbf{K}_{pp} \end{bmatrix} \begin{Bmatrix} \Delta U \\ \Delta P \end{Bmatrix} = \begin{Bmatrix} \Delta R \\ \Delta Q_f \end{Bmatrix} \quad (25)$$

where

$$\tilde{\mathbf{K}}_{uu} = \sum ([\tilde{\mathbf{k}}_{uu}]^{(e)}) \quad (26)$$

$$\mathbf{K}_{up} = \sum ([\mathbf{k}_{up}]^{(e)}) \quad (27)$$

$$[\mathbf{K}_{pp}] = \sum ([\mathbf{k}_p]^{(e)} + \vartheta \Delta t [\mathbf{k}_{pp}]^{(e)}) \quad (28)$$

$$\Delta R = \sum (\{\Delta f\}^{(e)} + \{\Delta R^p\}^{(e)} + \{\Delta R^c\}^{(e)} + \{\Delta R^d\}^{(e)}) \quad (29)$$

$$\{\Delta Q_f\} = \sum (\Delta t (\{Q_f\}^{(e)} + \vartheta \{\Delta Q_f\}^{(e)} - [\mathbf{k}_{pp}]^{(e)} \{p\}_n^{(e)})) \quad (30)$$

3.2. Numerical implementation

The integration scheme for the creep and seepage model is similar to that for the regular coupled HM model. Here the commercial software ABAQUS (ABAQUS, 2004) was used to solve the HM coupling problem. The following information is required to calculate the damage, permeability and deformation: (a) strain increment, (b) stress updating, (c) changes of damage and plastic variables, and (d) permeability evolution.

The procedure of interfacing UMAT subroutine with ABAQUS is listed as follows: (a) use ABAQUS to obtain the correction $\delta \mathbf{u}^{(n)}$ of the displacement increment $\Delta \mathbf{u}$ at time t_n by using equilibrium iteration; (b) calculate the strain increment $\Delta \epsilon$ based on the displacement-strain relationship; (c) the UMAT subroutine provides the stress tensor σ at time $t_n + \Delta t$ by using the given constitutive equation to ABAQUS; and (d) ABAQUS continues to step t_{n+1} if the results are convergent. The detailed procedure is given in Fig. 11:

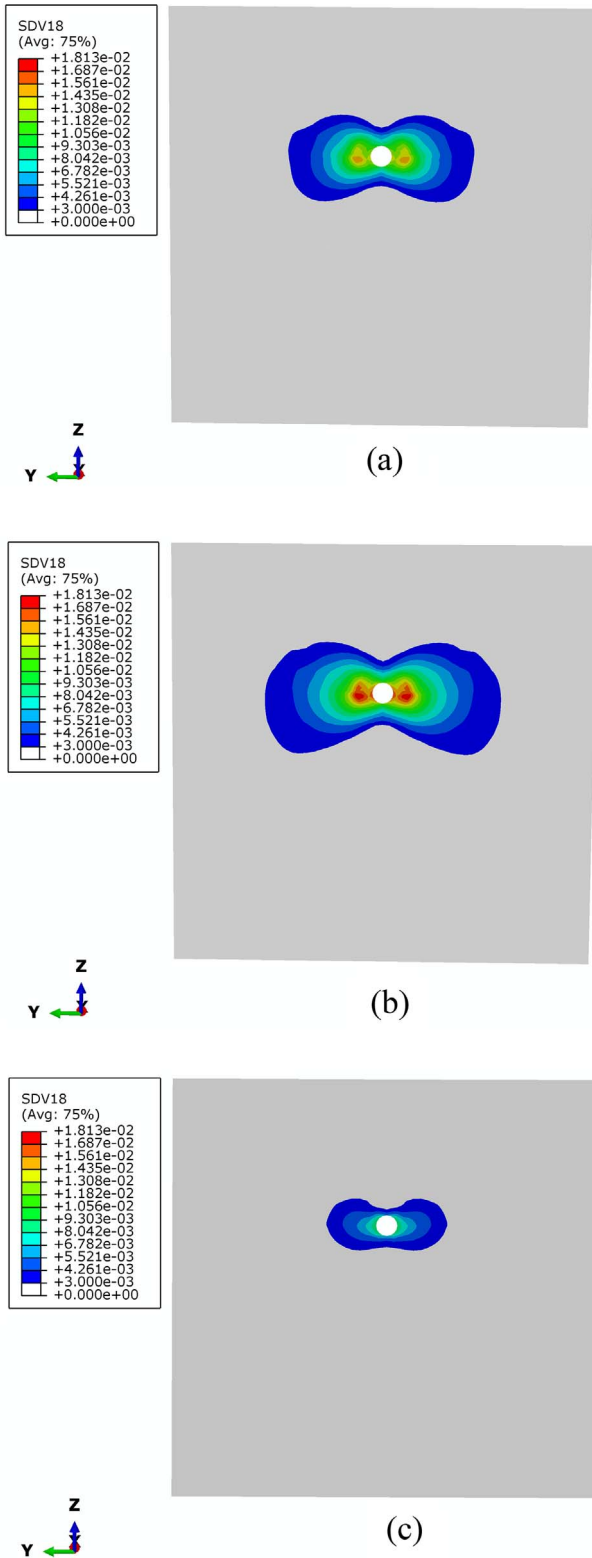


Fig. 20. Creep strain distribution around the drift for: (a) Section B-B (test drift) after 10 years, (b) Section B-B after 25 years and (c) Section C-C (connecting drift) after 10 years.

(1) At a given time t_n , ABAQUS provides stress tensor ${}^t_n\sigma$, total strain ${}^t_n\epsilon$, total strain increment ${}^t_n\Delta\epsilon$, and time increment Δt to the UMAT subroutine, which calculates the creep strain increment and stress by using the following equations (ABAQUS, 2004)

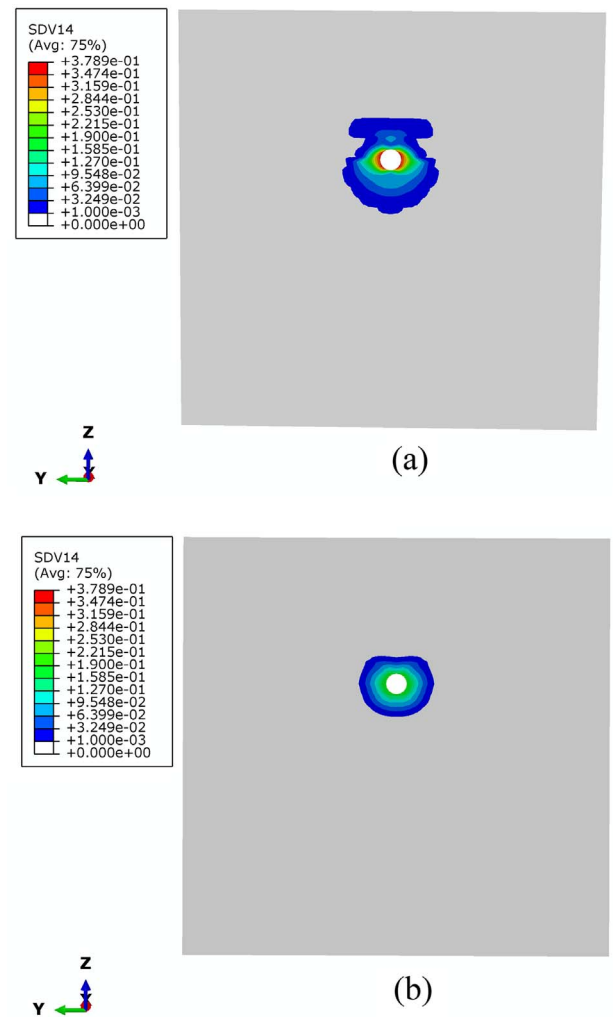


Fig. 21. Excavation damage distribution around the drift for (a) Section B-B and (b) Section C-C.

$$\begin{cases} \Delta\epsilon_c = \int_t^{t+\Delta t} d\epsilon_c = \int_t^{t+\Delta t} \frac{d\epsilon_c}{f^{cr}} \frac{\partial G}{\partial \sigma} d\tau \\ \Delta\epsilon_{ep} = \Delta\epsilon - \Delta\epsilon_c \\ \Delta\sigma = J\Delta\epsilon_{ep} \\ {}^{t_n+\Delta t}\sigma = {}^t_n\sigma + \Delta\sigma \end{cases} \quad (31)$$

where ${}^{t_n+\Delta t}\sigma$ is the updated stress at time $t_n + \Delta t$ and J is the Jacobian matrix. The damage value in the current step is assumed to be equal to that in the previous step.

(2) The stress ${}^{t_n+\Delta t}\sigma$ is substituted into yield criterion to determine the rock in elastic or plastic state. If the yield function is larger than zero, the Euler method is adopted to obtain the plastic parameter, plastic strain, and consistency matrix to ensure that the stress state is on the yield surface. To improve computational efficiency, the process of Aitken's Δ^2 is used to accelerate the iteration convergence (Kobayashi and Ohno, 2002). In each time step, the current plastic multiplier increment $\delta\lambda_{n+1}$ is replaced by the corrected one $\hat{\delta}\lambda_{n+1}$ every three iterations. The corrected plastic multiplier $\hat{\delta}\lambda_{n+1}$ is expressed as follows (Kobayashi and Ohno, 2002):

$$\hat{\delta}\lambda_{n+1} = \delta\lambda_{n+1}(i) - \frac{[\delta\lambda_{n+1}(i) - \delta\lambda_{n+1}(i-1)]^2}{\delta\lambda_{n+1}(i) - 2\delta\lambda_{n+1}(i-1) + \delta\lambda_{n+1}(i-2)}, \quad (i = 3, 6, 9, \dots) \quad (32)$$

where i is the number of iterations in the current increment. The condition for iterative convergence is

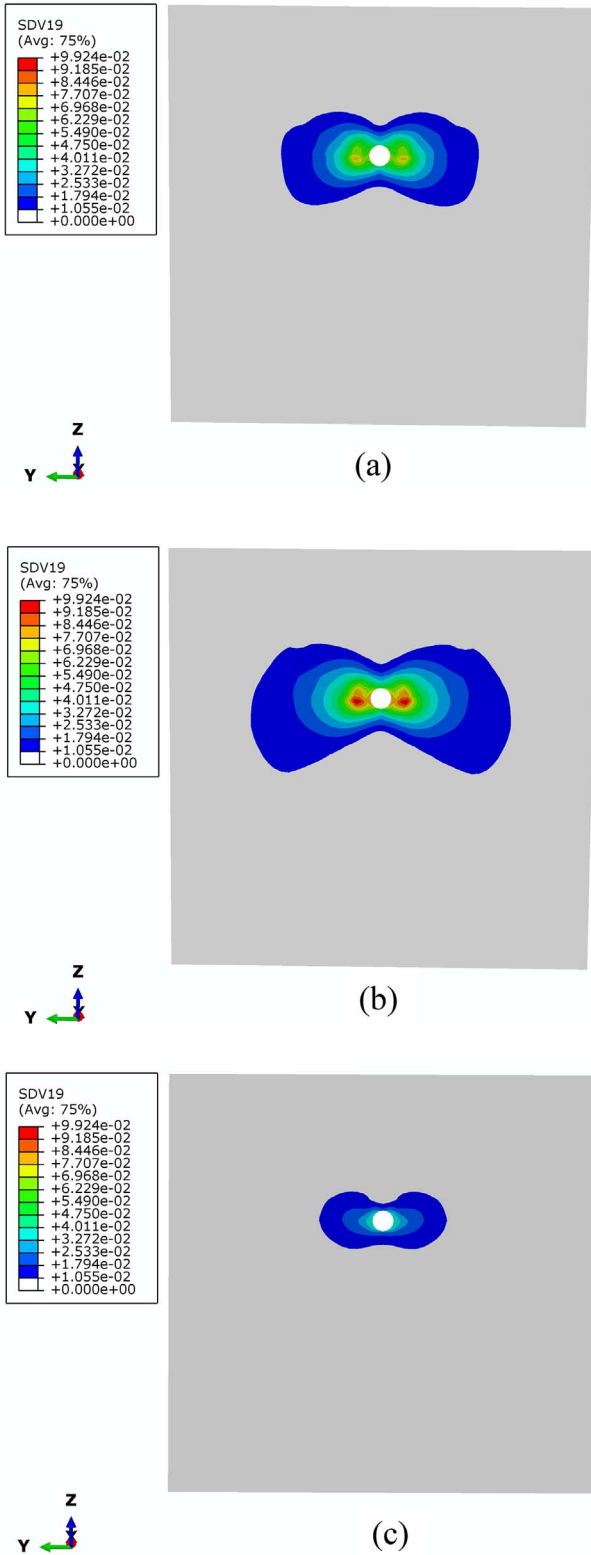


Fig. 22. Creep damage distribution around the drift for: (a) Section B-B after 10 years, (b) Section B-B after 25 years and (c) Section C-C after 10 years.

$$|1 - \delta\lambda_{n+1}(i-1) / \delta\lambda_{n+1}(i)| < 10^{-4} \quad (33)$$

(3) The strain is updated by

$${}^{t_n+\Delta t}\boldsymbol{\varepsilon} = {}^{t_n}\boldsymbol{\varepsilon} + \Delta\boldsymbol{\varepsilon} \quad (34)$$

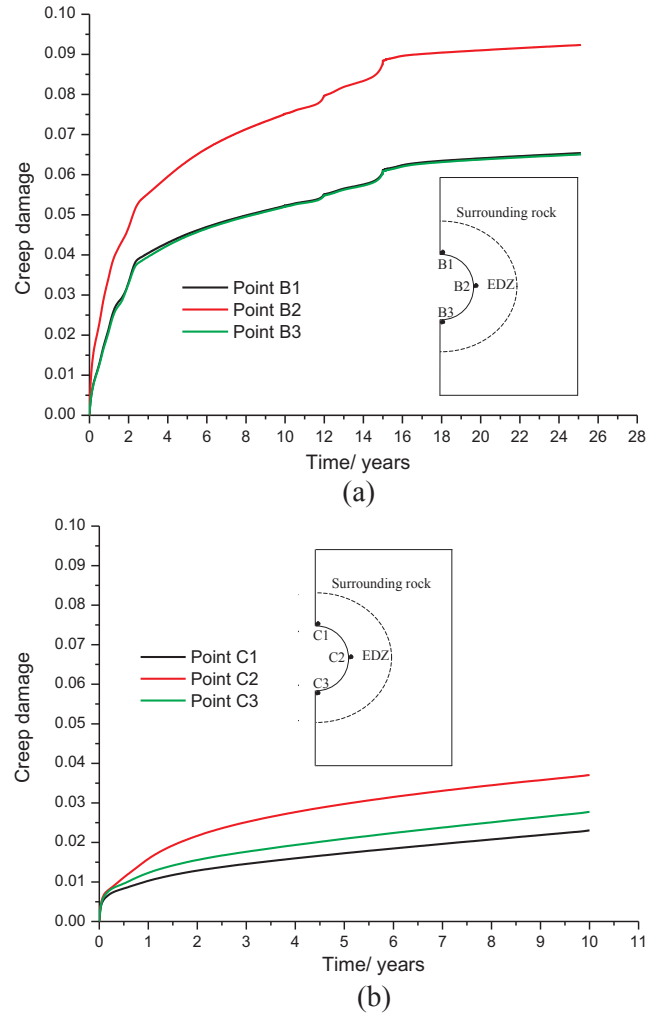


Fig. 23. Evolution of creep damage of the surrounding rock as a function of time for (a) Section B-B and (b) Section C-C.

The damage is determined according to elasto-plastic damage criterion given in Eq. (6) and creep damage criterion given in Eq. (9). Then, the current elasto-plastic damage and creep damage are replaced with ${}^{t_n+\Delta t}D_m$ and ${}^{t_n+\Delta t}D_c$, respectively.

- (4) A user defined subroutine USDFLD is used to calculate and update the permeability. The current permeability is obtained according to the current damages ${}^{t_n+\Delta t}D_m$ and ${}^{t_n+\Delta t}D_c$ and self-healing factor ${}^{t_n+\Delta t}h_s$.
- (5) At time t_{n+1} , the main routine of ABAQUS performs the equilibrium iteration using Newton–Raphson method. If the calculation is convergent, the program continues to the next time step; otherwise, the program reduces the time increment Δt until the calculation is convergent.

4. Application

In this section the proposed coupled creep and seepage model is applied to a particular case of a high-level radioactive waste repository in clayey rock.

4.1. Project profile

A high-activity disposal experimental site (HADES) is selected for investigating the HM properties of clayey rock and the feasibility of disposal of high-level radioactive waste, as shown in Fig. 12. Construction of the HADES contains the following stages (Barnichon and

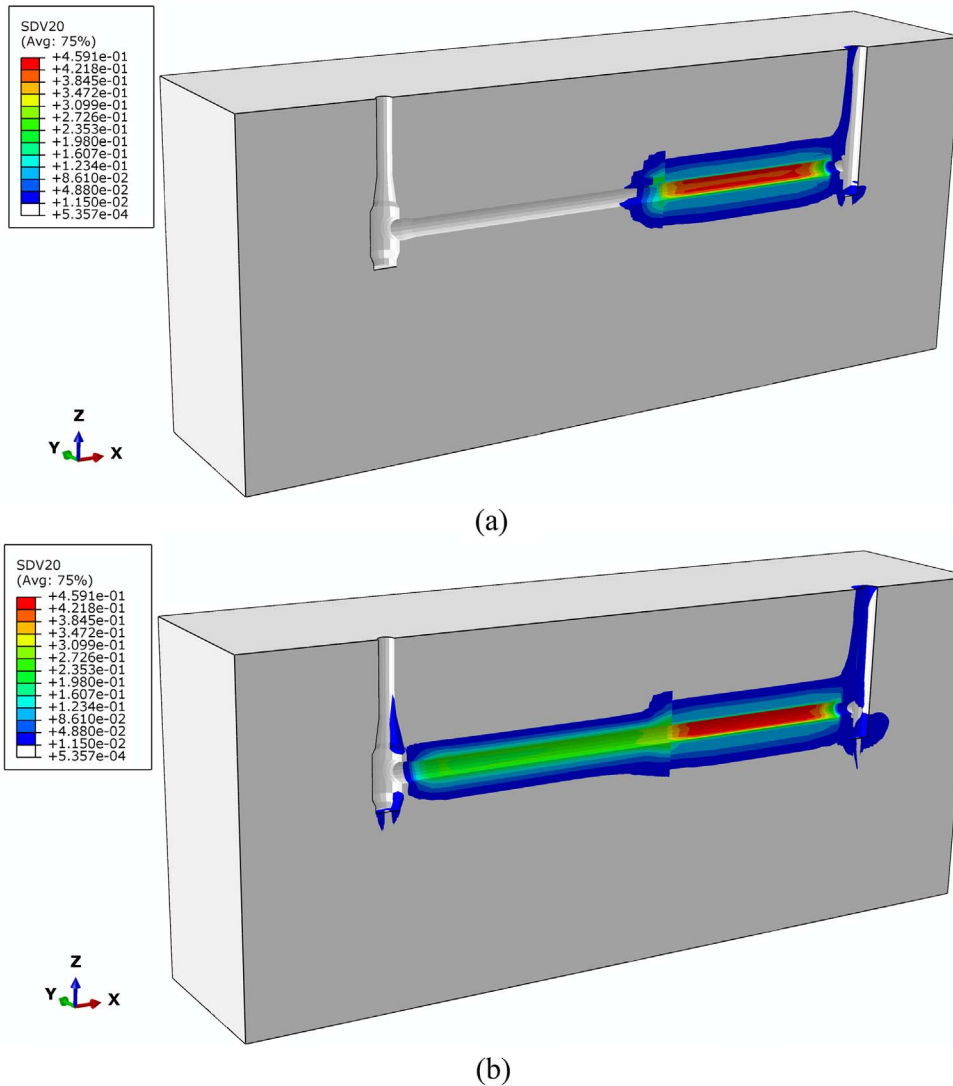


Fig. 24. Total damage distribution of HADES: (a) 10 years after the test drift was constructed and (b) 10 years after the connecting drift was constructed.

Volckaert, 2003; Bastiaens et al., 2007; Wileveau and Bernier, 2008; Jia, 2009). First, to ensure the geomechanical stability of the excavation, the first shaft was constructed in pre-frozen rock from 1980 to 1982. Freezing was provided by 2×16 frozen tubes evenly distributed in two concentric circles with diameters of 7 m and 13 m. Given the small excavation diameter of 4.3 m, the work was carried out using a pneumatic drill, with the spoil being raised in a large barrel that was used to carry men and machinery. Second, to prove the feasibility of excavating galleries with effective diameter of some 4 m in unfrozen clay, the excavation of test drift was carried out by hand using jackhammers, with a mean speed of 0.25 m/day in 1987. Third, the second shaft was constructed with a jackhammer mounted on the hydraulic arm and with manual air hammers from 1997 to 1999 in pre-frozen rock, where sixteen frozen holes were arranged in a 7 m diameter circle centered on the shaft axis. Fourth, in order to minimize the convergence and hence to limit the excavation-damaged zone, the connecting drift was constructed by shield tunneling method with a mean speed of 2 m/day in 2002.

Numerous instruments were placed in the gallery lining and the surrounding host rock since the operational start of HADES, but this study focuses on some representative set-ups allowing the long-term evolution of HM behaviour of clayey rock. The convergence measurements were carried out on the concrete lining segments of the test drift, recording the parameters relating to the long-term behaviour of the

host rock and lining. In order to study the EDZ of clayey rock, two sections of the connecting drift were equipped with multi-piezometers allowing long-term follow-up of pore pressures and measurement of the hydraulic conductivity. Fig. 12 shows the layout of these sections with robust and reliable data: (a) diametrical convergences of L43, L52, L83 and L105 in the test drift; (b) one upward (20 m, labelled L13) and one downward (40 m, labelled L55) piezometers installed in the connecting drift.

4.2. Computational condition

The initial vertical effective stress is 2.25 MPa and the lateral pressure coefficient is 0.85 (Jia, 2009). Both laboratory and field tests demonstrate that the permeability of clayey rock is anisotropic, and the horizontal permeability is larger than the vertical one (Li et al., 2011). As the permeability of clayey rock is very small, it is reasonable to assume that undrained conditions are imposed at the wall of the surrounding rock during excavation process. The mechanical properties of clayey rock are taken to be isotropic. The stress-strain curves under confining pressure 2.5 MPa are used to verify the mechanical damage parameters (Fig. 13). The creep tests are used to determine the creep parameters, and a comparison between simulation and testing results is shown in Fig. 14. The calculated parameters of clayey rock are shown in Table 1 (Barnichon and Volckaert, 2003; Bastiaens et al., 2007;

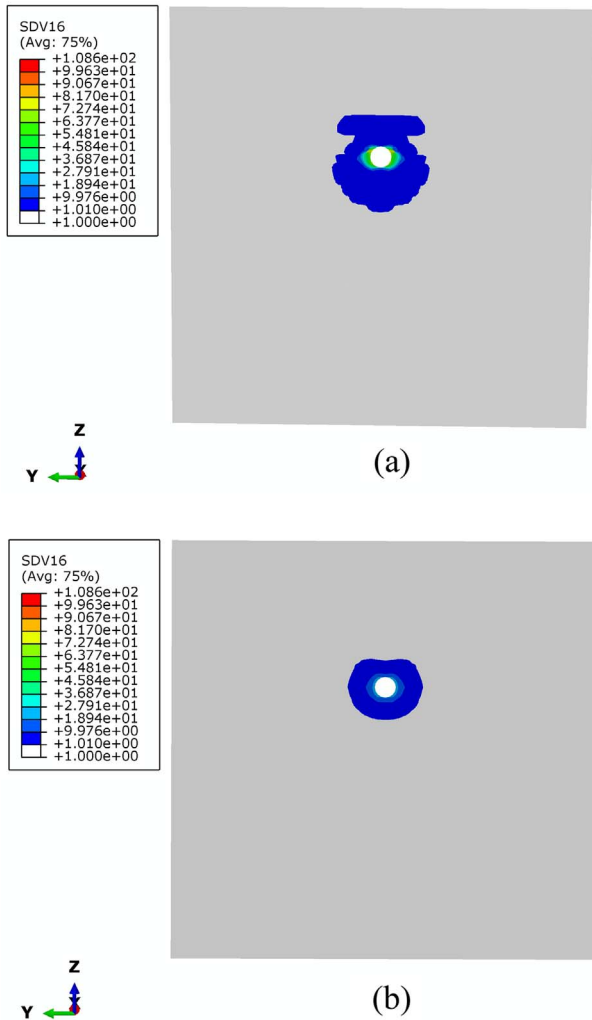


Fig. 25. Permeability distribution around the drift after excavation for (a) Section B-B and (b) Section C-C.

Wileveau and Bernier, 2008; Jia, 2009; Li et al., 2011).

The lining in the horizontal gallery is assumed to be elastic, and its stiffness is reduced because of the segment joints of lining. As its permeability is one order of magnitude larger than that of clayey rock, the drainage of lining must be considered. On the contrary, the shaft lining has a large width and good waterproofing ability, and thus the drainage of two shaft could be ignored. The material parameters for different linings are shown in Table 2.

The creep test on lining material shows that the concrete has an obvious non-linear viscoelasticity (Jia, 2009). To characterize effectively the long-term deformation of the gallery, the creep behaviour of lining should be considered. The elastic modulus, E , of concrete material is defined as a function of strain

$$E = E_0 - a_1 \varepsilon_0 - a_2 \varepsilon_c \quad (35)$$

where E_0 is the initial elastic modulus, a_1 and a_2 are material constants, ε_0 and ε_c are the instantaneous elastic strain and creep strain, respectively.

It is assumed that the non-linear viscoelasticity of lining is caused by the damage of the material. The damage variable for lining is defined as follows (Xie, 1990)

$$D_L = \frac{E_0 - E}{E_0} = \frac{a_1 \varepsilon_0 + a_2 \varepsilon_c}{E_0} \quad (36)$$

According to the results of creep tests on concrete material under a confining pressure close to the initial in-situ stress, the damage evolution equation based on the fitted curve shown in Fig. 15 is obtained

$$D_L = 0.03271t^{0.35318} \quad (37)$$

where t is time with a unit of day.

To simulate precisely the construction process of HADES including the first and second shaft, the test drift and connecting drift, the numerical model uses the actual size as shown in Fig. 16 and the simulation step is the same as the construction sequence in the real case. Because both the first and second shafts were constructed in the pre-frozen rock, release of in-situ stresses was ignored. The test drift was constructed by hand using jackhammers with an over-excavation radius of 20 cm. The connecting drift was constructed by using the shield tunneling method with an over-excavation radius of 4.5 cm.

4.3. Numerical results and discussion

The numerical analysis focused on the evolution of damage and permeability, transport of underground water, deformation of the surrounding rock, and lining convergence of the HADES. The number of the lining and layout of the survey line are shown in Fig. 12.

4.3.1. Numerical results

4.3.1.1. Creep deformation of the HADES. The deformation in the surrounding rock is shown in Figs. 17 and 18. It can be seen that the maximum displacement around the test drift is 7.312 cm when it was constructed, while that around the connecting drift is 3.983 cm when it was constructed. As the connecting drift is excavated by shield tunneling method, better construction quality and higher stiffness of lining segments make stress release and convergence of the surrounding rock less than those of the test drift. The creep effect is obvious for clayey rock with a maximum displacement of 9.590 cm around test drift after 10 years and 10.260 cm after 25 years. However, the maximum displacement around the connecting drift is 5.919 cm after 10 years.

Fig. 19 compares the convergent deformation of the lining in the test drift between the measured values and simulation results. As a result of the construction of the second shaft and connecting drift, the seepage field is disturbed, leading to changes in the creep condition of the surrounding rock and lining. It can be seen from Fig. 19 that the simulation results are in first order agreement with the testing data except that they fluctuated in the range of 10 to 15 years.

Fig. 20 shows the contour of the creep strain in the surrounding rock. The creep strain in the middle of Section B-B is much larger than that at the top and bottom, and the horizontal creep zone is larger than the vertical one. The maximum creep strain of the surrounding rock is 1.547% after 10 years and 1.813% after 25 years. The creep distribution of Section C-C is similar to that of Section B-B, but the maximum creep strain is 0.902% after 10 years. In addition, the creep strain and disturbed zone of the connecting drift is smaller than those of the test drift because of its good construction and lining qualities.

4.3.1.2. Damage evolution of the HADES. Fig. 21 shows the contour of the excavation damage in the surrounding rock. It is found that the damage around the test drift is larger than that around the connecting drift because of the influence of construction quality. The horizontal zone of damage is smaller than that of floor and roof around the test drift, whereas the damage zone around the connecting drift is almost round. The maximum damage around the test drift is approximately 0.379, while that around the connecting drift is about 0.204.

Fig. 22 displays the contours of creep damage in the surrounding rock and Fig. 23 presents the variations of creep damage with time at three points (roof, side wall and bottom of the drift) on Section B-B and Section C-C. It can be seen that (1) the creep damage in both sections increases rapidly at the early stage and tends to stabilize gradually; (2) the creep damage at the side wall of the drift is larger than that at the

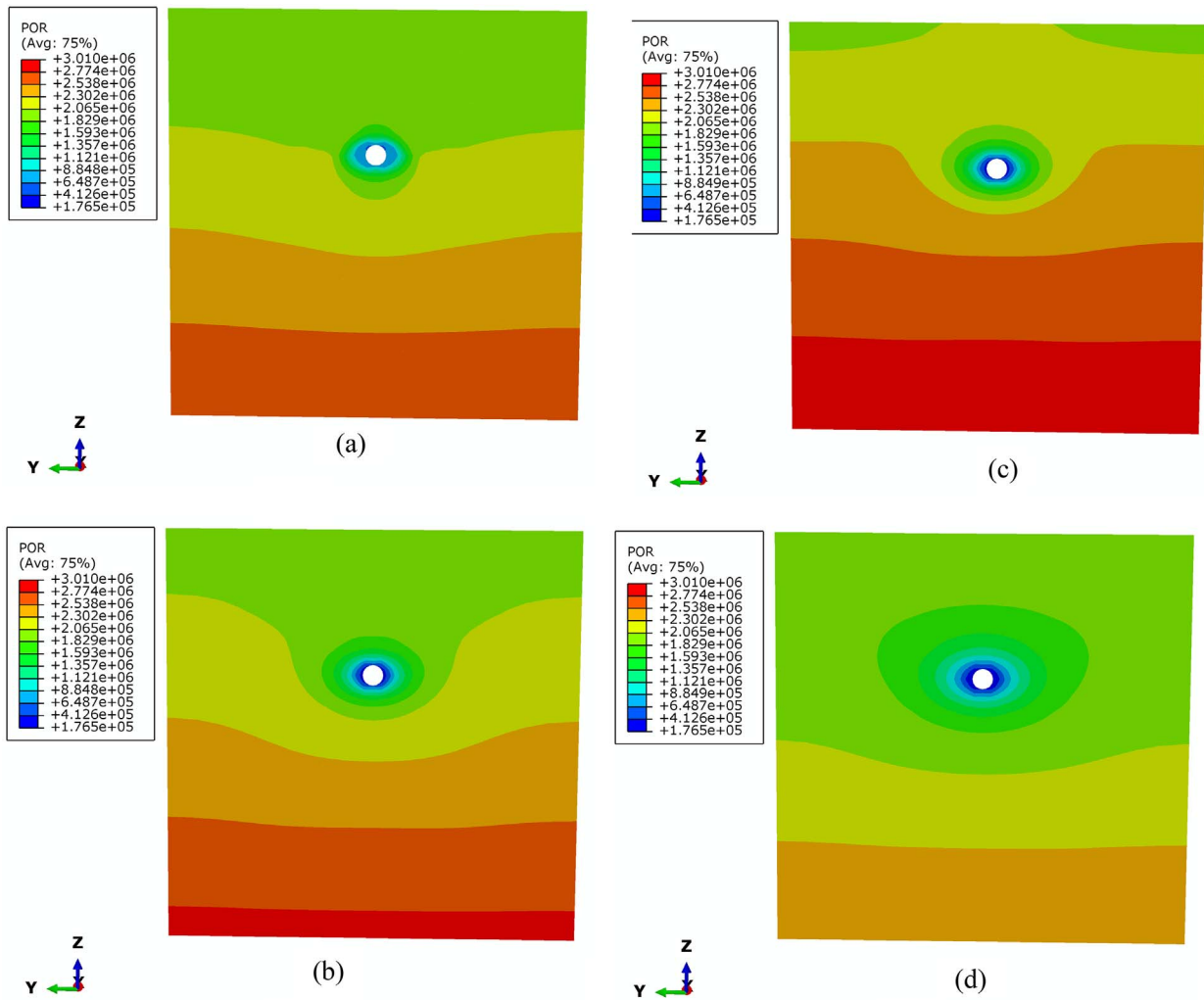


Fig. 26. Pore pressure variation with time in Section B-B around the drift: (a) after the test drift was constructed, (b) 10 years after the test drift was constructed (since 1987), (c) after the connecting drift was constructed and (d) 10 years after the connecting drift was constructed (since 2002).

roof and bottom of the drift; (3) the creep damage in Section B-B (with a maximum value of 0.079 and 0.099 after 10 and 25 years, respectively) is more serious than that in Section C-C (with a maximum value of 0.039 after 10 years).

The contour for the total damage of the HADES is plotted in Fig. 24, where the total damage around the test drift is larger than that around the connecting drift. The damage zone around the underground gallery expands gradually with creep damage. In addition, the creep damage around the second shaft is so small that it can be ignored, but the creep damage around the first shaft cannot be neglected from a long-term point of view.

4.3.1.3. Permeability evolution of the HADES. The contour for the permeability in the surrounding rock after excavation is shown in Fig. 25. It can be seen that the permeability of the EDZ around the test drift is larger than that around the connecting drift. The maximum permeability of the EDZ around the test drift is 108.6 times larger than that of the original clayey rock, while the maximum permeability around the connecting drift is 24 times larger than that of the original clay. The EDZ of the test drift has a larger radius (7.21 m) than that of connecting drift with a radius 3.98 m.

The contour for the pore pressure in the surrounding rock is shown in Figs. 26 and 27. The seepage field in the surrounding rock tends to be

steady state, and the pore pressure at the inner wall of gallery is smaller than that in the surround rock.

The permeability testing tools were set up in the L13 and L55 boreholes (Fig. 12), which are above and below the connecting drift, respectively. Fig. 28 compares the permeability in the disturbed zone between the numerical prediction and measured results (Bastiaens et al., 2007; Li et al., 2011). It can be found that they are in first order agreement, and the permeability along the given path varies in the same way. It has to be mentioned that, due to errors in upward testing, there exists a difference between the numerical and measured results when the measurement points are close to the tunnel wall, as shown in Fig. 28(b).

Fig. 29 shows the evolution of permeability with time at three points on the tunnel wall. Fig. 29(a) and (b) are for Section B-B (test drift) and Section C-C (connecting drift), respectively. The permeability at these three points increases rapidly after excavation and then it reaches a maximum value as a result of the creep damage effect. After that, it starts to decrease with time due to HM interaction and self-healing of fractures. After about three years, the permeability of the disturbed zone approaches that of the original clayey rock with an order of magnitude 10^{-19} m^2 , which is consistent with the field monitoring data (Bastiaens et al., 2007; Li et al., 2011).

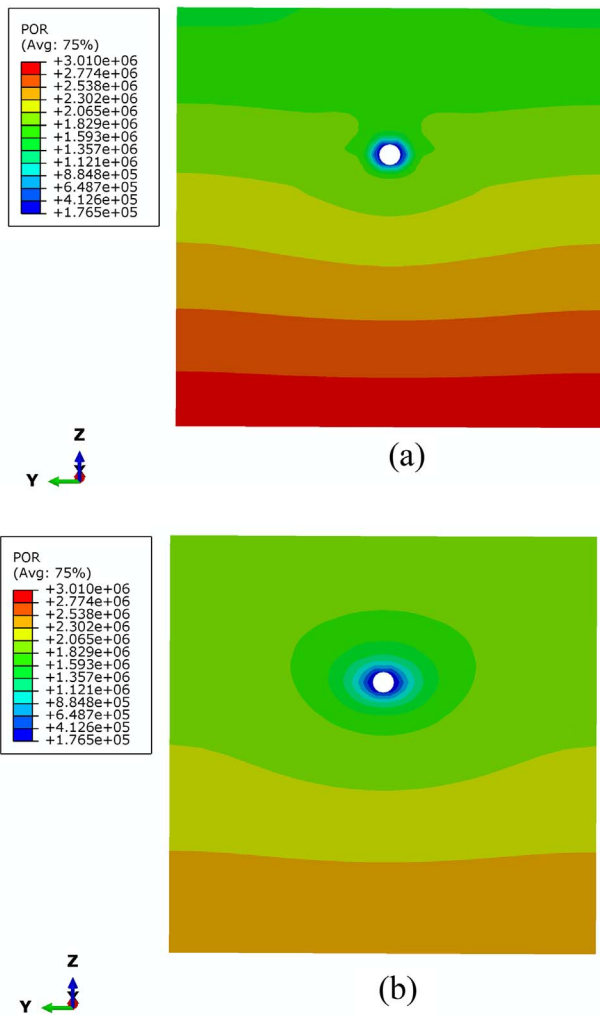


Fig. 27. Pore pressure variation with time in Section C-C around the drift: (a) after the connecting drift was constructed and (b) 10 years after the connecting drift was constructed (since 2002).

4.3.2. Discussion

In this work, it is assumed that the lining is isotropic and elastic. As for the lining around horizontal gallery, its physical characteristics is very complex because each ring around the test drift consists of 64 concrete blocks and 64 wooden plates, and each lining around the connecting drift is made of 10 segments. It should be noted that the nonlinear and discontinuous mechanical characteristics, and the coupled unsaturated water flow in concrete support and ventilation processes after excavation are beyond the scope of this paper. The present study focuses on modelling of creep and seepage coupling in clayey rock where the lining could be considered as in saturated state for long term response of the clayey rock.

The creation of EDZ is expected by using different construction methods, and the damage due to initiation and growth of macro- and micro-fractures has been observed (Mertens et al., 2004; Bastiaens et al., 2007). Our model shows that the permeability of EDZ increases very quickly after excavation and then decreases gradually with time after lining support, which agrees with the in situ observations (Bastiaens et al., 2007; Li et al., 2011; Jia et al., 2015). In the EDZ, the permeability of clayey rock decreases gradually with the distance away from the tunnel wall. The excavation damage does trigger significant increases of permeability due to unloading, but the permeability change of transient excavation is different from that of creep damage effect. The self-healing of macro- and micro-fractures in clayey rock is a combined

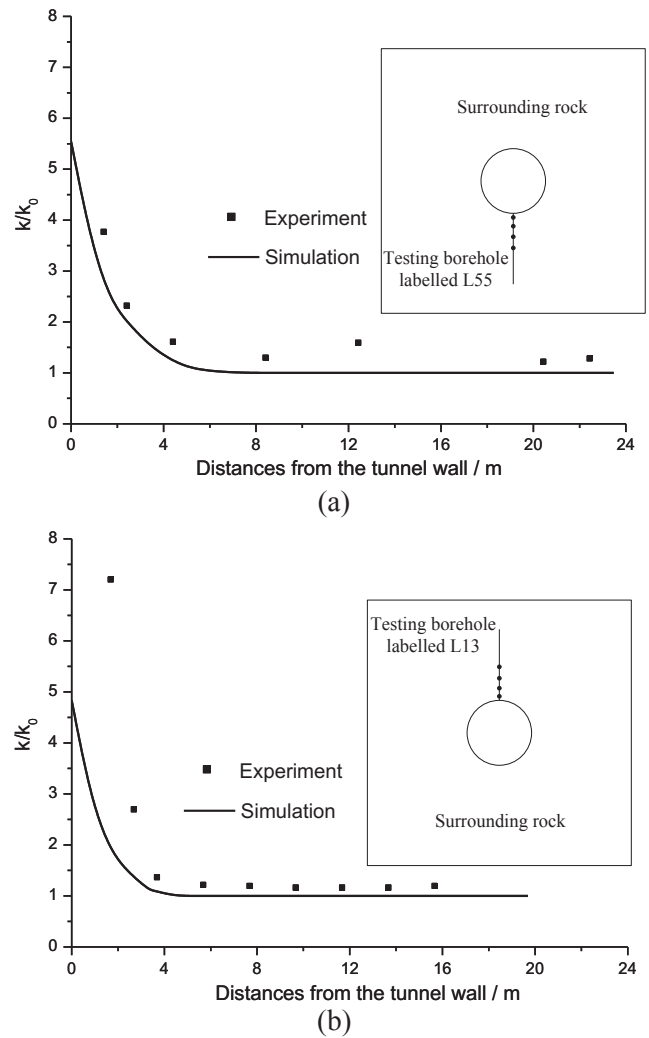


Fig. 28. Comparison of permeability between numerical and measured results: (a) connecting drift, L55 drill down and (b) connecting drift, L13 drill up.

result of creep deformation and seepage which requires special stress state, fluid flow and saturated time through long term coupling. Due to lack of experimental data about the effect of fracture self-healing on the mechanical properties and creep damage, the mechanical parameters and creep parameters are assumed to be independent of the self-healing effect in this study. Therefore, further work on the coupled process of self-healing and creep behaviour in clayey rock is required in the future as it is of great importance for the studying the safety issue of the nuclear waste repository.

5. Conclusions

Based on laboratory experiments and field tests on excavation disturbed zone, a new viscoelastic-plastic creep model was developed by using a modified Mohr–Coulomb criterion, in which the damage evolution equations is dependent on the relationship between damage and strain. The proposed model can explain the damage mechanism of hardening, softening behaviours and creep deformation of clayey rock. The permeability equations of clayey rock were constructed with emphasis on the damage and self-healing processes.

The construction quality has a considerable effect on the excavation disturbed zone (EDZ) of the surrounding rock. The shape of EDZ is almost round with good construction quality. The creep damage of the surrounding rock increases rapidly in the early stage and tends to

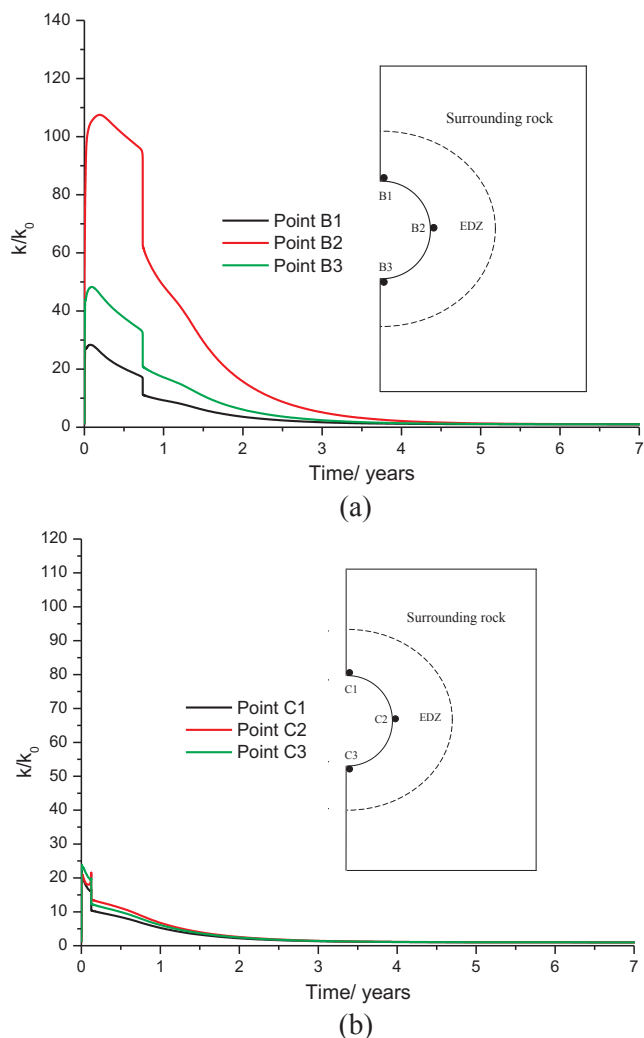


Fig. 29. Evolution of permeability ratio of the surrounding rock as a function of time for (a) Section B-B and (b) Section C-C.

stabilize gradually. The damage of the middle part of the surrounding rock is larger than that of the bottom and top parts. The permeability of EDZ increases after excavation and tends to self-heal with time. Approximately three years later, the permeability of EDZ is close to that of the original clayey rock. The proposed coupled creep and seepage model can effectively explain the initial permeability increase caused by excavation and creep damage, and the subsequent permeability decrease resulting from the self-healing effect of clayey rock.

Acknowledgments

The authors gratefully acknowledge the support of the Open Research Fund of State Key Laboratory of Geomechanics and Geotechnical Engineering, Institute of Rock and Soil Mechanics, Chinese Academy of Sciences (Grant No. Z013007), the Natural Science Foundation of Hubei Province, China (Grant No. 2015CFB194) and the National Natural Science Foundation of China (Grant No. 51379200).

References

ABAQUS, 2004. Analysis User's Manual, Version 6.5.
 Barnichon, J.D., Volckaert, G., 2003. Observations and predictions of hydromechanical coupling effects in the Boom clay, Mol Underground Research Laboratory, Belgium. *Hydrogeol. J.* 11, 193–202.
 Bastiaens, W., Bernier, F., Li, X.L., 2007. SELFRAC: experiments and conclusions on fracturing, self-healing and self-sealing processes in clays. *Phys. Chem. Earth* 32,

600–615.
 Chiarelli, A.S., Shao, J.F., Hoteit, N., 2003. Modeling of elastoplastic damage behavior of a claystone. *Int. J. Plast.* 19, 23–45.
 Cristescu, N.D., Hunsche, U., 1998. *Time Effects in Rock Mechanics*. Jone Wiley & Sons Ltd.
 Elkhoury, J.E., Detwiler, R.L., Ameli, P., 2015. Can a fractured caprock self-heal? *Earth Planet. Sci. Lett.* 417, 99–106.
 Fabre, G., Pellet, F., 2006. Creep and time-dependent damage in argillaceous rocks. *Int. J. Rock Mech. Min. Sci.* 43, 950–960.
 Fan, Q.Y., Yang, K.Q., Wang, W.M., 2010. Study of creep mechanism of argillaceous soft rocks. *Chinese J. Rock Mech. Eng.* 29 (8), 1555–1561 (in Chinese).
 Gasc-Barbier, M., Chanchole, S., Bérest, P., 2004. Creep behavior of Bure clayey rock. *Appl. Clay Sci.* 26, 449–458.
 Giraud, A., Rousset, G., 1996. Time-dependent behaviour of deep clays. *Eng. Geol.* 41, 181–195.
 Gong, Z., 2015. Long-term thermo-hydro-mechanical coupled behaviour of Belgium Boom clay. PhD Thesis. University of Chinese Academy of Sciences, China.
 Hou, Z., Lux, K.H., 2004. A new coupling concept for the hydro-mechanical interaction of clay stone and rock salt in underground waste repositories. In: Paper 2B 40-SINOROCK2004 Symposium.
 Hou, Z.M., 2003. Mechanical and hydraulic behavior of rock salt in the excavation disturbed zone around underground facilities. *Int. J. Rock Mech. Min. Sci.* 40, 725–738.
 Hunsche, U., Hampel, A., 1999. Rock salt—the mechanical properties of the host rock material for a radioactive waste repository. *Eng. Geol.* 52, 271–291.
 Jia, S.P., 2009. Hydro-mechanical coupled creep damage constitutive model of boom clay, back analysis of model parameters and its engineering application. PhD Thesis. Wuhan Institute of Rock & Soil Mechanics, Chinese Academy of Sciences, China (in Chinese).
 Jia, S.P., Chen, W.Z., Yang, J.P., Chen, P.S., 2010. An elastoplastic constitutive model based on modified Mohr-Coulomb criterion and its numerical implementation. *Rock Soil Mech.* 31 (7), 2051–2058 (in Chinese).
 Jia, S.P., Gong, J., Gao, M., Luo, J.Z., Yu, H.D., 2015. Inversion analysis of permeability coefficients of excavation-disturbed zone around a mudstone roadway with considering self-healing effect. *Rock Soil Mech.* 36 (5), 1444–1454 (in Chinese).
 Kobayashi, M., Ohno, N., 2002. Implementation of cyclic plasticity models based on a general form of kinematic hardening. *Int. J. Numer. Meth. Eng.* 53, 2217–2238.
 Kolditz, O., Shao, H., Wang, W.Q., Bauer, S., 2015. *Thermo-Hydro-Mechanical-Chemical Processes in Fractured Porous Media: Modelling and Benchmarking*. Springer, Switzerland.
 Labiouse, V., Giraud, A., 1998. Analytical solutions for the undrained response of a poro-elasto-plastic medium around a cylindrical opening. In: Thimus, J.F. (Ed.), *Poromechanics*. Balkema, Rotterdam, pp. 439–444.
 Li, Y., Matej, G., Isabelle, W., 2011. Boom clay hydraulic conductivity: a synthesis of 30 years of research report. Mol: SCK-CEN.
 Lisjak, A., Garitte, B., Grasselli, G., Müller, H.R., Vietor, T., 2015. The excavation of a circular tunnel in a bedded argillaceous rock (Opalinus Clay): short-term rock mass response and FDEM numerical analysis. *Tunn. Undergr. Space Technol.* 45, 227–248.
 Liu, W., Li, Y.P., Yang, C.H., Daemen, J., Yang, Y., Zhang, G.M., 2015. Permeability characteristics of mudstone cap rock and interlayers in bedded salt formations and tightness assessment for underground gas storage caverns. *Eng. Geol.* 193, 212–223.
 Mertens, J., Bastiaens, W., Dehandschutter, B., 2004. Characterisation of induced discontinuities in the Boom Clay around the underground excavations (URF, Mol, Belgium). *Appl. Clay Sci.* 26, 413–428.
 Millard, A., Maßmann, J., Rejeb, A., Uehara, S., 2009. Study of the initiation and propagation of excavation damaged zones around openings in argillaceous rock. *Environ. Geol.* 57, 1325–1335.
 Muñoz, J.J., 2006. Thermo-hydro-mechanical analysis of soft rock: application to a large heating test and large scale ventilation test. PhD Thesis. Universitat Politècnica De Catalunya.
 Pardo, B., Levasseur, S., Collin, F., 2015. Using local second gradient model and shear strain localisation to model the excavation damaged zone in unsaturated claystone. *Rock Mech. Rock Eng.* 48, 691–714.
 Rejeb, A., 2003. Time-dependent behaviour of Tournemire argillites (France). ISRM 2003–Technology roadmap for rock mechanics. South African Institute of Mining and Metallurgy.
 Renner, J., Hettkamp, T., Rummel, F., 2000. Rock mechanical characterization of an argillaceous host rock of a potential radioactive waste repository. *Rock Mech. Rock Eng.* 33 (3), 153–178.
 Rutenberg, M., Lux, K.H., 2011. Numerical simulation of the time-dependent deformation behaviour of claystone rock mass at the Tournemire site with 2D and 3D models. *Phys. Chem. Earth* 36, 1913–1921.
 Souley, M., Armand, G., Su, K., Ghoreychi, M., 2011. Modeling the viscoplastic and damage behavior in deep argillaceous rocks. *Phys. Chem. Earth* 36, 1949–1959.
 Tian, H.M., Chen, W.Z., Yang, D.S., Gong, Z., 2015. Experimental and numerical analysis of the time-dependent behaviour of argillaceous red sandstone under high in situ stress. *Bull. Eng. Geol. Environ.* 74, 567–575.
 Wang, R.B., Xu, W.Y., 2013. Coupling relation between damage-induced permeability evolution and accelerated creep deformation of volcanic breccias. In: Feng, Hudson, Tan (Eds.), *Rock Characterisation, Modelling and Engineering Design Methods*. Taylor & Francis Group, London.
 Wileveau, Y., Bernier, F., 2008. Similarities in the hydromechanical response of Callovo-Oxfordian clay and Boom Clay during gallery excavation. *Phys. Chem. Earth* 33, S343–S349.
 Xie, H.P., 1990. *Damage Mechanics of Rock and Concrete*. China University of Mining and Technology Press.
 Xu, W.Y., Wang, R.B., Wang, W., Zhang, Z.L., Zhang, J.C., Wang, W.Y., 2012. Creep

- properties and permeability evolution in triaxial rheological tests of hard rock in dam foundation. *J. Central South Univ.* 19, 252–261.
- Yang, S., Jing, H., Cheng, L., 2014. Influences of pore pressure on short-term and creep mechanical behavior of red sandstone. *Eng. Geol.* 179, 10–23.
- Yu, H.D., Chen, W.Z., Gong, Z., Tan, X.J., Ma, Y.S., Li, X.L., Sillen, X., 2015. Creep behavior of boom clay. *Int. J. Rock Mech. Min. Sci.* 76, 256–264.
- Yu, H.D., Chen, W.Z., Jia, S.P., Cao, J.J., Li, X.L., 2012. Experimental study on the hydro-mechanical behavior of Boom clay. *Int. J. Rock Mech. Min. Sci.* 53, 159–165.
- Zhang, C.L., Rothfuchs, T., 2004. Experimental study of the hydro-mechanical behaviour of the Callovo-Oxfordian argillite. *Appl. Clay Sci.* 26, 325–336.
- Zhang, C.L., Rothfuchs, T., 2008. Damage and sealing of clay rocks detected by measurements of gas permeability. *Phys. Chem. Earth* 33, S363–S373.